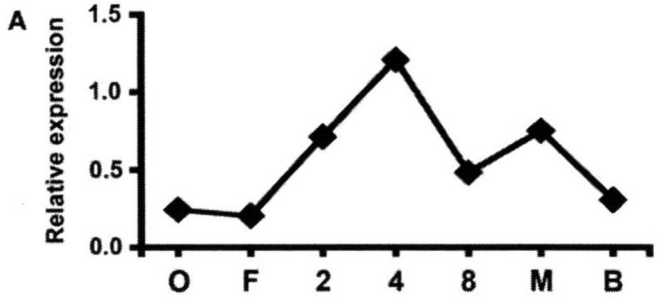

B

Develpmental stage	Gene EST	Total EST in pool
Oocyte	0	19488
Unfertilized ovum	0	20366
Zygote	0	28382
Cleavage	16	65852
Blastocyst	0	69938
Egg cylinder	0	12257
Gastrula	0	28673
Organogenesis	0	128591
Fetus	0	670244
Neonate	0	107177
Juvenile	0	293396
Adult	0	1026072

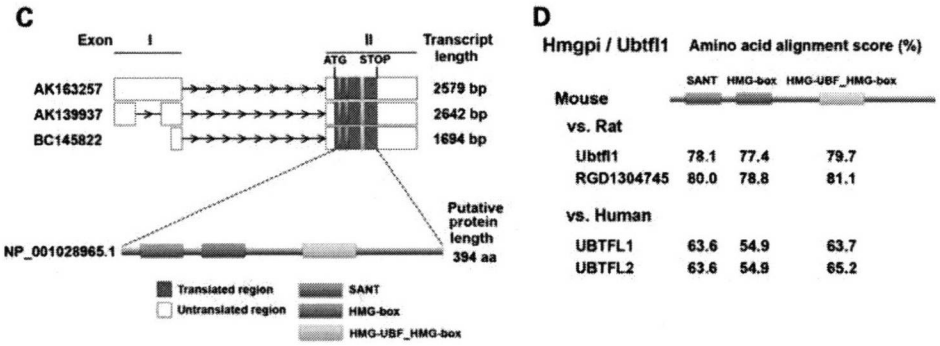

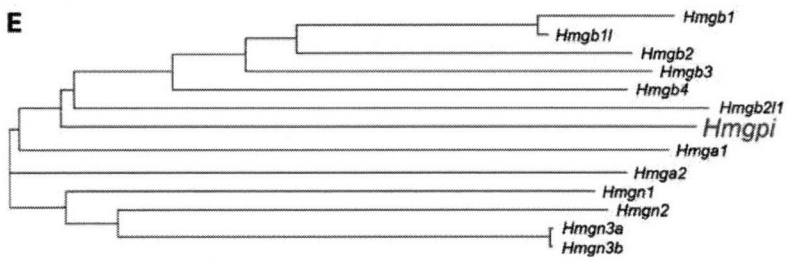

Figure 1. *In silico* analysis of *Hmgpi* expression. (**A**) Previous microarray analysis of *Hmgpi* expression. *Hmgpi* expression appeared at the 2-cell stage, peaked at the 4-cell stage and then decreased (3). (**B**) Expression sequence tag (EST) frequencies in Unigene cDNA libraries. Out of 4.7 million mouse ESTs, 16 *Hmgpi* clones were exclusively detected at the cleavage stages: 9, 2 and 5 ESTs from 2-cell, 4-cell and 8-cell libraries, respectively. (**C**) Exon–intron structures and a putative protein structure of *Hmgpi*. *Hmgpi* has three exon–intron models and one protein model. Predicted protein domains are also shown. (**D**) Conserved domains of *Hmgpi*/*Ubtfl1* gene in mouse, rat and human. Pairwise alignment scores of conserved domains between species were shown. (**E**) Phylogenetic tree of gene nucleotide acid sequences containing HMG domains determined by a sequence distance method and the neighbour-joining (NJ) algorithm (41) using Vector NTI software (Invitrogen, Carlsbad, CA, USA).

stage (Fig. 2A). Furthermore, significant expression of *Hmgpi* was detected in ES cells, although not in embryonic carcinoma (EC) cells nor in mesenchymal stem cells (Fig. 2B). The relative abundance of *Hmgpi* transcripts in preimplantation embryos was measured by real-time quantitative RT–PCR (qRT–PCR) analysis (Fig. 2C). Four independent experiments were conducted with four replicates of 10 embryos each. To normalize the qRT–PCR reaction efficiency, *H2afz* was used as an internal standard (20). *Hmgpi* mRNA levels increased during the 1- to 2-cell stage, peaked at the 4-cell stage, and then gradually decreased during the 8-cell to blastocyst stage (Fig. 2C). The *in silico*-predicted preimplantation-stage-specific expression pattern of *Hmgpi* was therefore validated.

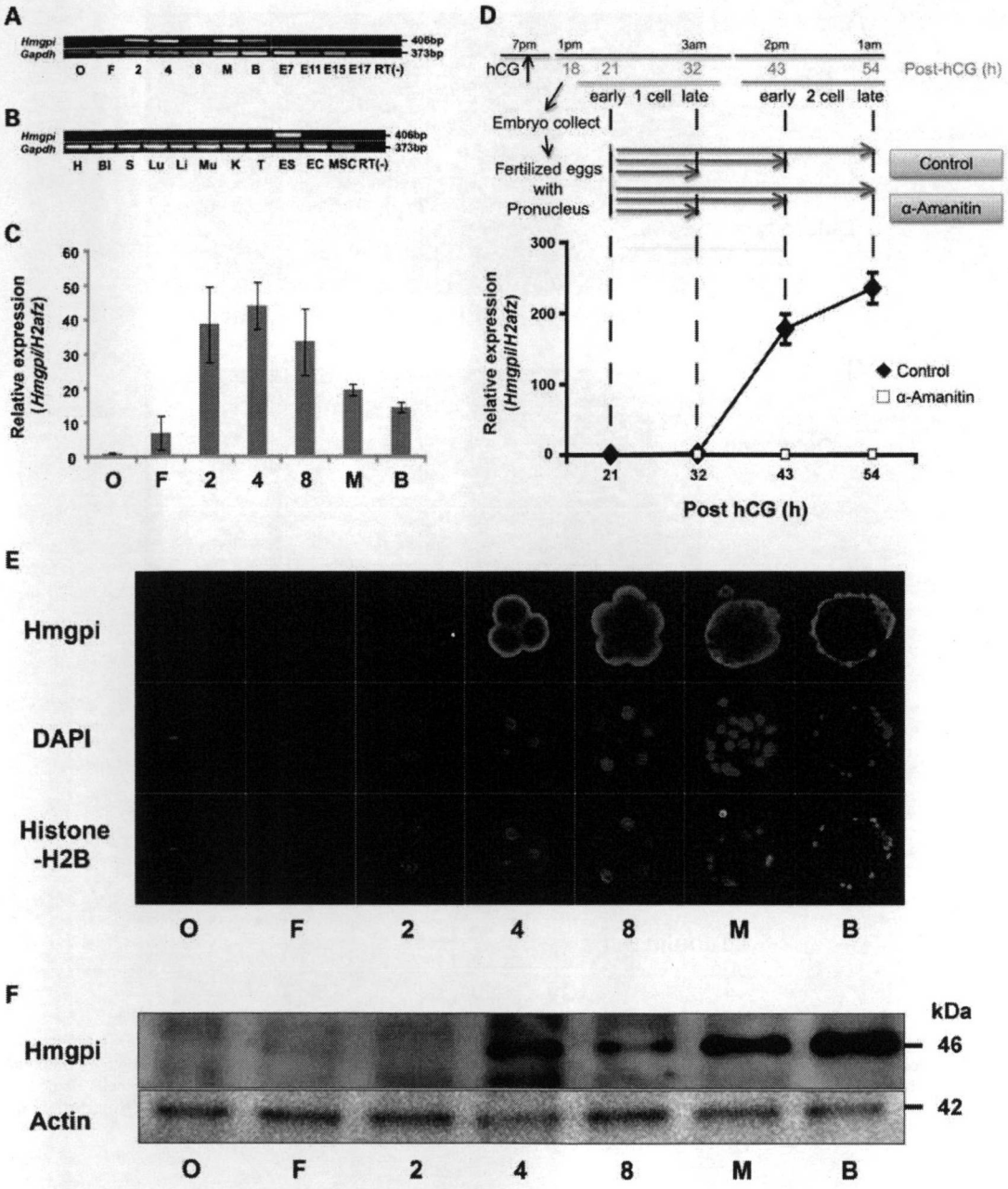

Figure 2. Expression of *Hmgpi* in preimplantation embryos and other tissues. (**A**) RT–PCR analysis of *Hmgpi* expression during preimplantation and postimplantation development (E7–E17). Three sets of 10 pooled embryos were collected from each stage (O: oocyte, F: fertilized egg, 2: 2-cell embryo, 4: 4-cell embryo, 8: 8-cell embryo, M: morula, and B: blastocyst) and used for RT–PCR analysis. The predicted sizes of the PCR products of *Hmgpi* and *Gapdh* are 406 and 373 bp, respectively. No PCR products were detected in the no-RT negative control (4-cell embryo). (**B**) RT–PCR analysis of *Hmgpi* expression in adult tissues, ES cells, EC cells and mesenchymal stem cells. mRNA was isolated from mouse tissues (H: heart, Bl: bladder, S: spleen, Lu: lung, Li: liver, Mu: muscle, K: kidney, T: testis, ES: ES cells, EC: EC cells, and MSC: mesenchymal stem cells). No PCR products were detected in the no-RT negative control (ES cells). (**C**) Real-time quantitative RT–PCR analysis of *Hmgpi* expression during preimplantation development. Fold differences in amounts of *Hmgpi* mRNA from the same numbers of oocytes (O), fertilized eggs (F), 2-cell embryos (2), 4-cell embryos (4), 8-cell embryos (8), morulae (M) and blastocysts (B) are shown after normalization to an internal reference gene (mouse *H2afz*). Values are means ± SE from four separate experiments. (**D**) *De novo* (zygotic) transcription of the *Hmgpi* gene. α-Amanitin studies revealed that *Hmgpi* is transcribed zygotically, but not maternally. *Hmgpi* expression was not observed before the 2-cell stage and α-amanitin completely inhibited *de novo* transcription at the 2-cell stage (closed rhombus: control group, open square: α-amanitin-treated group). The expression levels were normalized using *H2afz* as a reference gene. Values are means ± SE from four separate experiments. (**E**) Immunocytochemical analysis of HMGPI expression. MII oocytes and preimplantation embryos were immunostained with an anti-HMGPI antibody (red) and an anti-Histone-H2B antibody as a positive control of nuclear staining (green). Nuclei are shown by DAPI staining (blue). HMGPI protein was detected from 4-cell embryos to blastocysts. (**F**) Immunoblot analysis of HMGPI during preimplantation development. An amount of extracted protein corresponding to 100 oocytes or embryos was loaded per lane. Actin was used as a loading control. The representative result is shown from three independent experiments.

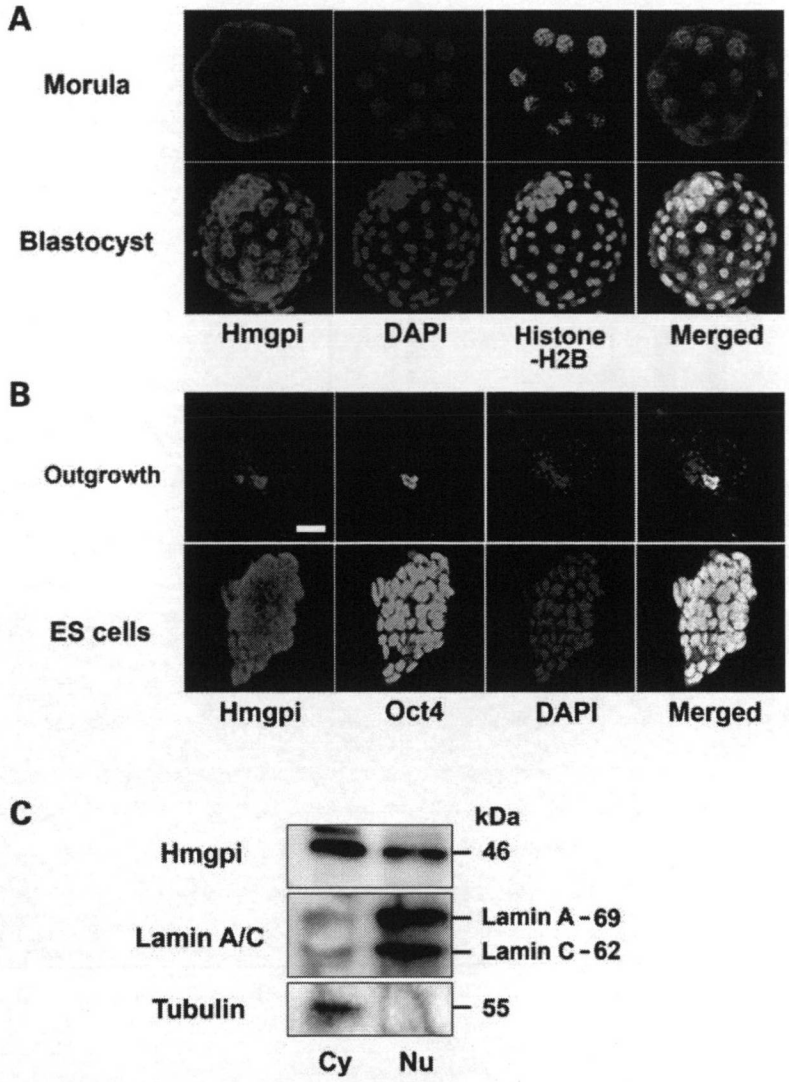

Figure 3. Localization of HMGPI in preimplantation embryos. (**A**) Nuclear translocation of HMGPI protein at the blastocyst stage. HMGPI was mainly detected in the cytoplasm of preimplantation embryos (from 4-cell embryos to morulae), but in the nuclei of blastocysts. Nuclei are shown by immunostaining with an anti-Histone-H2B antibody (green) and DAPI staining (blue). (**B**) Confocal microscopy images of blastocyst outgrowth and ES cells stained with antibodies to *Hmgpi* and *Oct4*, and with DAPI. Scale bar = 50 μM. (**C**) Western blotting analysis of HMGPI in cytoplasmic (Cy) and nuclear (Nu) fractions of ES cells. Lamin A/C and tubulin were used as markers of the nuclear and cytoplasmic fractions, respectively.

We then performed qRT–PCR analysis using α-amanitin to investigate *de novo* (zygotic) transcription of the *Hmgpi* gene. The supplementation of α-amanitin during *in vitro* culture from the 1-cell stage significantly reduced *Hmgpi* mRNA expression in the 2-cell embryos at post-hCG 43 and 53 h (early and late 2-cell stage, respectively) (Fig. 2D), implying that *Hmgpi* is transcribed zygotically during the major burst of ZGA, but not maternally.

To study the temporal and spatial expression pattern of the *Hmgpi*-encoded protein (HMGPI), we raised a polyclonal antibody against *Hmgpi* peptides. Western blot analysis of extracts from the mouse blastocysts showed only a single band corresponding to 46 kDa detected by the anti-HMGPI antibody. In addition, preincubation with the HMGPI peptide antigen abolished detection of the HMGPI protein, while preincubation with a control peptide had no effect on the immunodetection (Supplementary Material, Fig. S1). Although *Hmgpi* transcription started at the 2-cell stage, peaked at the 4-cell stage and then gradually decreased until the blastocyst stage (Fig. 2C), immunostaining and immunoblotting analysis revealed HMGPI expression from the 4-cell stage until the blastocyst stage, indicating a delayed expression pattern of HMGPI compared with that of the *Hmgpi* transcript. It was also notable that both ICM cells and trophectodermal cells retained HMGPI expression in blastocysts.

On the other hand, immunostaining for HMGPI in preimplantation embryos showed a unique subcellular localization pattern. Although a putative nuclear protein due to its role

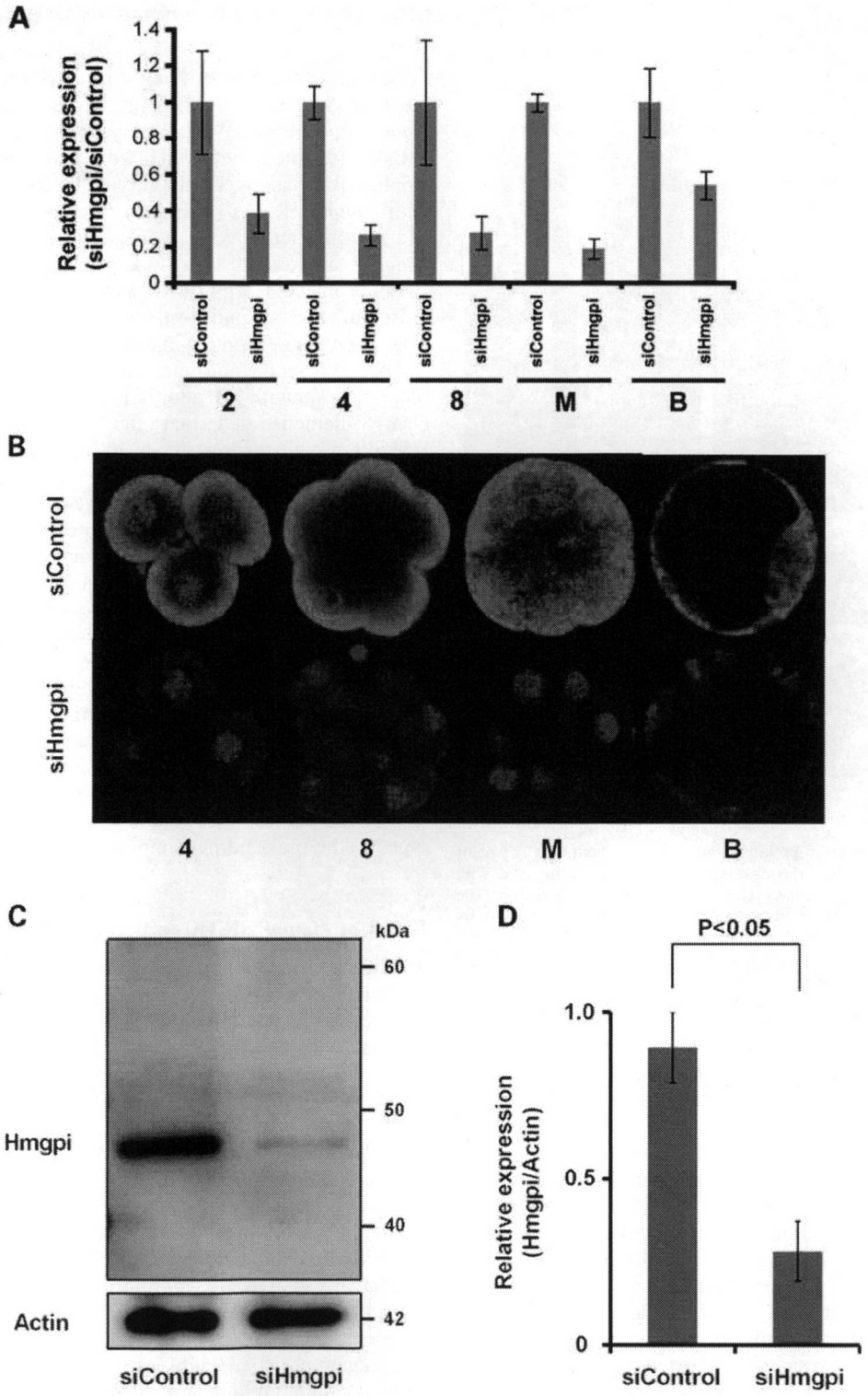

Figure 4. Loss-of-function study by siRNA technology. (**A**) Transcript levels of *Hmgpi* in embryos injected with control siRNA (siControl) and *Hmgpi* siRNA (siHmgpi) by real-time quantitative RT–PCR analysis. The expression levels were normalized using *H2afz* as a reference gene. Values are means ± SE for four separate experiments. (**B**) Laser scanning confocal microscopy images of HMGPI protein expression in a 4-cell embryo, 8-cell embryo, morula and blastocyst after injection with siControl or siHmgpi (red, HMGPI; blue, chromatin). (**C** and **D**) Immunoblot analysis of HMGPI expression at the blastocyst stage in siControl-injected and siHmgpi-injected embryos. The relative amount of HMGPI (46 kDa) was determined at the blastocyst stage (left: siControl-injected embryos, right: siHmgpi-injected embryos). The expression levels were normalized using actin expression (42 kDa) as a reference. Values are means ± SE from three separate experiments.

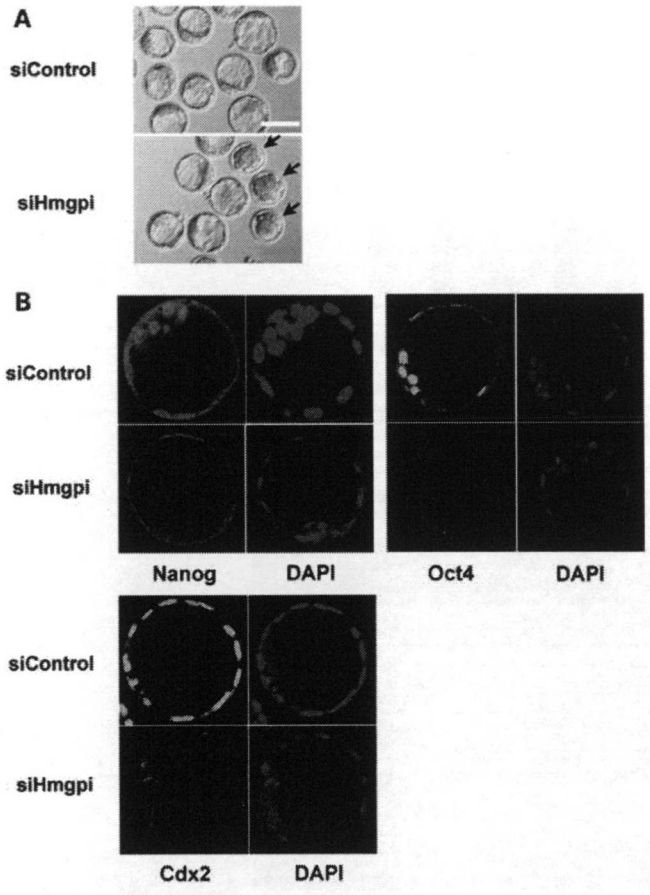

Figure 5. Function of *Hmgpi* in preimplantation development. (**A**) A pair of representative photos showing the development of embryos injected with *Hmgpi* siRNA (siHmgpi) and Control siRNA (siControl). The siHmgpi-injected embryos arrested at the morula stage are indicated by arrows. Scale bar = 100 μM. (**B**) For Nanog, Oct4 and Cdx2 immunostaining, all blastocysts in the siHmgpi-injected and siControl-injected groups were processed simultaneously. The laser power was adjusted so that the signal intensity was below saturation for the developmental stage that displayed the highest intensity and all subsequent images were scanned at that laser power. This allowed us to compare signal intensities for Nanog, Oct4 and Cdx2 expression between the siHmgpi-injected and siControl-injected embryos (Supplementary Material, Table S2).

as a transcription factor, HMGPI was detected mainly in the cytoplasm without any evidence of a nuclear localization from the 4-cell to the morula stage, suggesting a role other than transcriptional regulation (Fig. 2E). In contrast, HMGPI was localized to the nuclei rather than to the cytoplasm of blastocysts (Figs 2E and 3A). During blastocyst outgrowth, HMGPI was expressed in the nuclear region of most outgrowing cells, with scant amounts detected in the cytoplasm (Fig. 3B). Interestingly, Oct4-positive cells derived from the ICM showed particularly strong positive staining for HMGPI in the nucleus, suggesting a specific role as a nuclear protein in ES cells (Fig. 3B). On more closely examining HMGPI in ES cells, we found that almost all the Oct4-positive undifferentiated ES cells in a colony also expressed HMGPI (Fig. 3B), and immunoblotting confirmed HMGPI expression in both nuclear and cytoplasmic fractions of ES cells (Fig. 3C).

Effect of siRNA on *Hmgpi* mRNA level and protein synthesis

To investigate a role of *Hmgpi* in early embryonic development, we knocked down *Hmgpi* expression in mouse preimplantation embryos. We employed an oligonucleotide-based siRNA (denoted here siHmgpi and obtained from PE Applied Biosystems, Foster City, CA, USA). Zygotes injected with *Hmgpi* siRNAs (siHmgpi) or control siRNA (siControl) and non-injected zygotes as negative controls were cultured. *Hmgpi* expression was severely suppressed in the siHmgpi-injected embryos, and significantly lower than those in the siControl-injected or non-injected embryos (Fig. 4A). The siControl-injected embryos did not show any difference from the non-injected embryos in *Hmgpi* expression (data not shown). In addition, immunofluorescent staining clearly demonstrated that the siRNA injection reduced HMGPI protein expression in an individual preimplantation embryo (Fig. 4B). In the same set of experiments, the HMGPI levels were also assayed by western blotting (Figs 4C and 4D). HMGPI expression was significantly reduced in siHmgpi-injected blastocysts (0.89 ± 0.10) compared with that in negative controls (0.28 ± 0.08; $P < 0.05$).

Furthermore, we confirmed that siHmgpi had no influence on the expression of other genes with sequence similarities to *Hmgpi*, namely *Ubtf*, *Hmgb1*, *Hmgb2* and *Hmgb3*. Although *Ubtf*, *Hmgb1*, *Hmgb2* and *Hmgb3* were all expressed in control preimplantation embryos, the siHmgpi construct used in this study did not affect the expression of these genes in the siHmgpi-injected embryos (Supplementary Material, Fig. S2). On the other hand, it has been demonstrated that loss-of-function of these genes produces no distinct phenotypes at the pre- and peri-implantation stages (21).

Effect of *Hmgpi* siRNA on preimplantation development

To study the function of *Hmgpi* during preimplantation development, siHmgpi-injected or siControl-injected zygotes were cultured *in vitro* until the blastocyst stage. The embryos injected with siHmgpi at 21–23 h after hCG administration often failed to become blastocysts at 3.5 days postcoitum (dpc) (Fig. 5A). In addition, the reduction in Hmgpi expression significantly suppressed preimplantation development, whereby $68.9 \pm 1.3\%$ of siHmgpi-injected embryos became blastocysts, while $94.1 \pm 1.3\%$ of siControl-injected embryos reached the blastocyst stage (Supplementary Material, Fig. S3; $P < 0.0001$). Most of the siHmgpi-injected embryos that failed to become blastocysts showed developmental arrest after the morula stage and did not appear to form blastocoels, suggesting impairment of trophectodermal development (Supplementary Material, Fig. S3). To analyze the phenotype of siHmgpi-injected embryos further, we performed immunofluorescence staining of lineage-specific markers such as Cdx2, Nanog and Oct4 at the blastocyst stage. Although siHmgpi-injected embryos that reached the blastocyst stage appeared morphologically intact, the expression of lineage-specific markers was reduced (Fig. 5B). Cdx2, which is required for implantation and extra-embryonic development, was particularly and markedly down-regulated in trophectodermal cells, while Nanog and Oct4

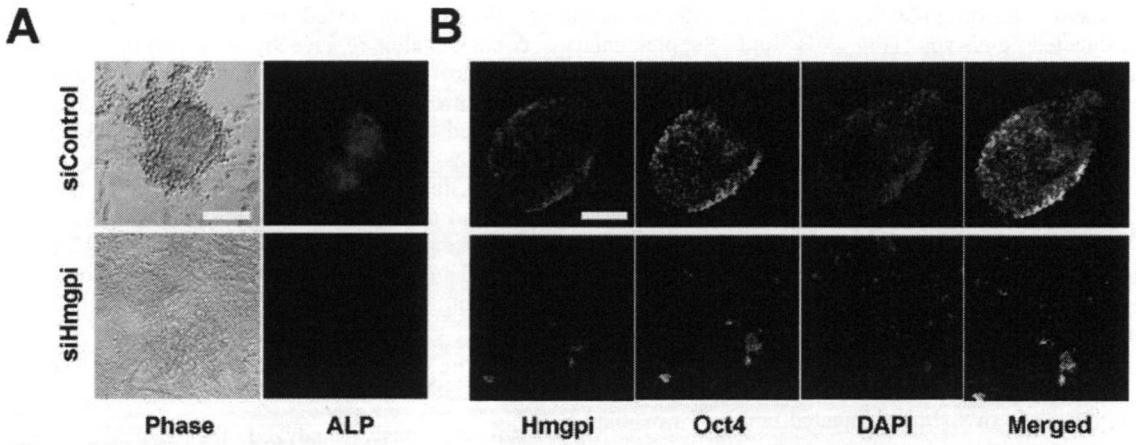

C

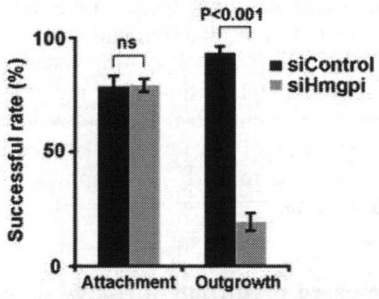

	Tested blastocysts	Attachment (%)	Outgrowth (%)
siControl	51	34 (66.6)	30 (88.2)
siHmgpi	20	15 (75.0)	2 (13.3)
siControl	117	92 (78.6)	80 (86.9)
siHmgpi	13	10 (76.9)	2 (20.0)
siControl	55	49 (89.0)	48 (97.9)
siHmgpi	8	7 (87.5)	1 (14.2)
siControl	41	33 (80.4)	33 (100.0)
siHmgpi	13	10 (76.9)	3 (30.0)

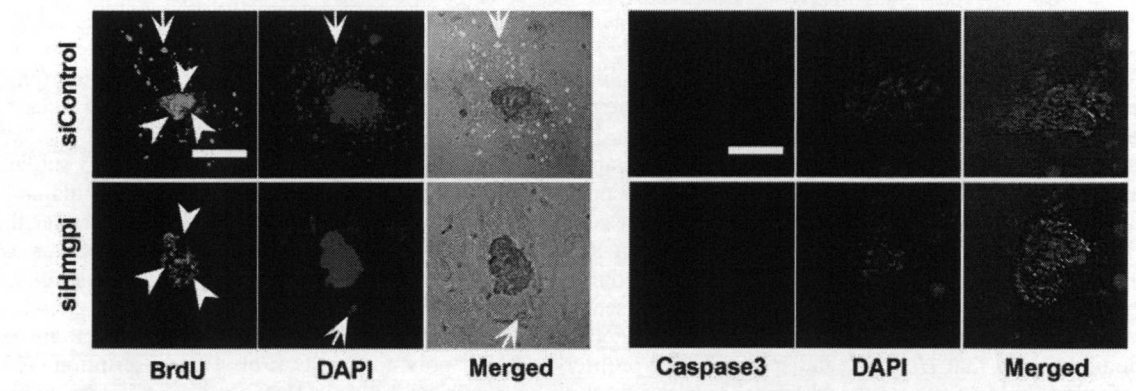

F

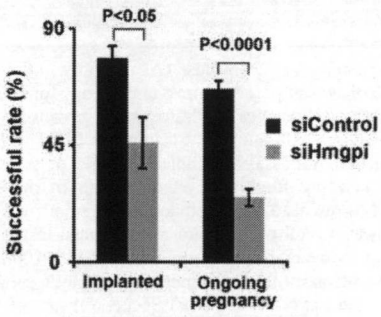

	Transferred embryos	Implanted (%)	Ongoing pregnancy (%)
siControl	30	23 (76.7)	20 (66.7)
siHmgpi	18	6 (33.3)	3 (16.7)
siControl	30	25 (83.3)	18 (60.0)
siHmgpi	32	20 (62.5)	10 (31.2)
siControl	16	13 (81.2)	12 (75.0)
siHmgpi	24	15 (62.5)	7 (29.1)
siControl	20	13 (65.0)	13 (65.0)
siHmgpi	32	8 (25.0)	7 (21.8)

were likewise downregulated in ICM cells of the siHmgpi-injected embryos (Fig. 5B and Supplementary Material, Table S2). Thus, *Hmgpi* is essential for the earliest embryonic development; both ICM and trophectodermal development.

Effect of *Hmgpi* siRNA on *in vivo* and *in vitro* peri-implantation development

To investigate the role of *Hmgpi* in proliferation of the ICM and trophectodermal cells, siHmgpi-injected and siControl-injected embryos were further cultured *in vitro* from the blastocyst stage, and attachment and outgrowth of each embryo on gelatin-coated culture plates was examined. HMGPI expression in siHmgpi-injected embryos was significantly reduced, and immunostaining showed that many colonies of ICM cells in the embryos collapsed during outgrowth culture (Fig. 6A and B). Although the vast majority of ICMs from siControl-injected embryos showed successful attachment (80.3 $\pm$ 4.9%) and vigorous outgrowth (96.2 $\pm$ 2.7%), those from siHmgpi-injected embryos failed to proliferate or produced only a residual mass (19.3 $\pm$ 3.8%) despite successfully attaching (79.0 $\pm$ 2.8%) (Fig. 6C; attachment ns; outgrowth, $P < 0.001$). These results implied that *Hmgpi* is essential for proliferation of ICM and trophectodermal cells in peri-implantation development, and for derivation of ES cells.

We then investigated cell proliferation and apoptosis during blastocyst outgrowth. Comparable incorporation of BrdU in blastocyst outgrowths of siHmgpi-injected embryos was less than that of siControl-injected embryos. Proliferation was significantly reduced in ICM-derived cells and dramatically suppressed in trophoblast cells (Fig. 6D). Embryonic fibroblasts were used as a feeder layer in this study and could support ICM cells, thus proliferation should have proceeded regardless of trophectodermal cell support. Therefore, the collapsed ICM-derived colonies in the current experiment were not a secondary effect of reduced proliferation in trophoblast cells, but a direct effect of the siHmgpi-induced decrease in ICM proliferation. Apoptosis was not detected in any cells during blastocyst outgrowth of siHmgpi-injected embryos, based on the absence of active caspase3 (Fig. 6E). Taken together, these findings show that *Hmgpi* is indispensable for proliferation of the ICM and trophectodermal cells in peri-implantation development and for the generation of ES cells.

Finally, we tested whether the experimental blastocysts could develop *in vivo* by transferring siHmgpi-injected and siControl-injected blastocysts into the uterus of pseudopregnant mice. Only 45.8 $\pm$ 9.7 and 24.7 $\pm$ 3.3% of blastocysts injected with siHmgpi implanted and developed, respectively, whereas most of the siControl-injected embryos showed successful implantation and ongoing development (76.5 $\pm$ 4.0 and 66.6 $\pm$ 3.3%, respectively) (Fig. 6F; implanted, $P < 0.05$; ongoing pregnancy, $P < 0.0001$). These results confirmed a role for *Hmgpi* in peri-implantation embryonic development.

DISCUSSION

We previously analyzed the dynamics of global gene expression changes during mouse preimplantation development (3). Understanding these preimplantation stages is important for both reproductive and stem cell biology. Many genes showing wave-like activation patterns (e.g. ZGA and MGA) during preimplantation were identified, and any or all of these may contribute to the complex gene regulatory networks. *Hmgpi*, one of the few novel preimplantation-specific genes, is involved in early development, implantation and ES cell derivation.

Structure-based prediction of *Hmgpi* function

Structural information about a protein sometimes hints at functional mechanisms, which remain unknown for *Hmgpi*'s clear role in early embryonic development. The HMG family proteins are abundant nuclear proteins that bind to DNA in a non-sequence-specific manner, influence chromatin structure and enhance the accessibility of binding sites to regulatory factors (17). Based on the number and the type of HMG domains, *Hmgpi* is relevant to the HMGB subfamily, characterized by containing two HMG-box domains ('HMG-box' or 'HMG-UBF_HMG-box'), rather than either the HMGA or HMGN subgroups. *Hmgpi* is also known as *Ubtfl1* in the NCBI gene database, based on sequence similarity to *Ubtf*, a well-known ZGA gene (3,22). *Ubtf*, encoding a SANT domain and six HMG-box domains, functions exclusively in RNA polymerase I (Pol I) transcription (23) and acts through its multiple HMG boxes to induce looping of DNA, which creates a nucleosome-like structure to modulate tran-

Figure 6. Function of *Hmgpi* in peri-implantation development. (**A**) Blastocyst outgrowth and alkaline phosphatase (AP) activity in the siHmgpi-injected and siControl-injected embryos, carried out according to a standard procedure (42). Representative images of phase-contrast microscopy for blastocyst outgrowth and fluorescent immunocytochemistry for AP are shown. Scale bar = 100 μM. (**B**) Confocal microscopy images of blastocyst outgrowth for the siHmgpi-injected and siControl-injected embryos, stained with antibodies to Hmgpi and Oct4. Nuclei are shown by DAPI staining. Scale bar = 100 μM. (**C**) Successful rate of blastocyst outgrowth for siHmgpi-injected and siControl-injected embryos. Successful outgrowth in this assay was indicated by the presence of proliferating cells after 6 days in culture. The experiment was repeated four times. (**D**) BrdU incorporation assay for blastocyst outgrowth of the siHmgpi-injected and siControl-injected embryos. Cell proliferation was determined by BrdU incorporation (ICM: arrowhead, trophectodermal cells: arrow). The trophectodermal component contained few cells and BrdU incorporation was confined to the ICM core; however, cell proliferation was reduced in the blastocyst outgrowth of siHmgpi-injected embryos compared with that of the siControl-injected embryos. Nuclei are shown by DAPI staining. Scale bar = 100 μM. (**E**) Immunocytochemistry with an anti-caspase3 antibody in blastocyst outgrowth of the siHmgpi-injected and siControl-injected embryos. Apoptotic cells were not apparent in the blastocyst outgrowth of either injected embryo. Nuclei are shown by DAPI staining. Scale bar = 100 μM. (**F**) Successful rate of siHmgpi-injected and siControl-injected embryo transfer. We transferred 3.5 dpc blastocysts into the uteri of 2.5 dpc pseudopregnant ICR female mice. The pregnant ICR mice were sacrificed on day 12.5 of gestation and the total numbers of implantation sites and of live and dead embryos/fetuses were counted. The experiment was repeated four times.

scription of the 45S precursor of ribosomal RNA (rRNA) by Pol I (24,25). Because the association of UBTF with rRNA genes *in vivo* is not restricted to the promoter and extends across the entire transcribed portion, UBTF promotes the formation of nucleolar organizer regions, indicative of 'open' chromatin (26). Based on the sequence similarity between UBTF and HMGPI, HMGPI might also bind to DNA in a non-specific manner, and modulate chromatin during peri-implantation when dynamic chromatin change is essential.

Alternatively, HMGPI may act as a cytokine during preimplantation development in a similar manner to HMGB1. HMGB proteins are found primarily in the cell nucleus, but also to varying extents in the cytosol (27,28), and have been suggested to shuttle between compartments (17). HMGB1 is indeed passively released from nuclei upon cell death and actively secreted as a cytokine (29), and the addition of recombinant HMGB1 into culture medium enhances *in vitro* development of mouse zygotes to the blastocyst stage in the absence of BSA supplementation (30). Although HMGPI failed to be detected in culture media after *in vitro* culture of preimplantation embryos or ES cells in this study (data not shown), two different modes of Hmgpi action, chromatin modulator and secreted mediator, should be taken into consideration as discussed later.

Role of *Hmgpi* during peri-implantation

The HMGPI protein was first detected in 4-cell embryos and then abundantly expressed in 8-cell embryos, morulae, ICM, trophectoderm and ES cells. Although *Hmgpi* transcription peaked at the 4-cell stage, the most dramatic siRNA effect appeared at the blastocyst and subsequent stages. This discrepancy between temporal expression and phenotype is attributed to three possible mechanisms. First, protein expression is generally delayed from transcription, indicated here by the *Hmgpi* transcripts and HMGPI protein expression peaking at the 4-cell stage and blastocyst stage, respectively. Similarly, *Stella* (31) and *Pms2* (32) are maternal-effect genes, but do not cause developmental loss until later preimplantation stages. A second possibility is the incompleteness of siRNA knockdown. One limitation of such knockdown experiments is the potential variability in levels of silencing of a target gene, which could in turn underlie the observed phenotypic variability in the present study. Embryos with complete suppression of Hmgpi may exhibit developmental arrest at earlier stages (e.g. at the morula stage), while those with less suppression may not display a phenotype until the later stages (e.g. at the implantation stage). Ideally, the suppression level of each embryo could be experimentally analyzed to correlate with the phenotype. The third possibility is spatial translocation of HMGPI protein in the blastocyst cells. The HMGPI expression pattern indicated differential spatial requirements during early embryogenesis, supported by the apparent ability of HMGPI to shuttle between the nucleus and the cytoplasm; the cytoplasmic HMGPI observed from the 4-cell to morula stages and the nuclear HMGPI in blastocysts and ES cells could have different functions. A bipartite nuclear localization signal (NLS) peptide (FKKEKEDFQKKMRQFKK) similar to NLS of HMGN2/HMG-17 (33) is also present in the HMGPI sequence. Thus, the nuclear HMGPI in blastocysts and ES cells might exert a critical transcriptional role to regulate gene expression essential for peri-implantation development. Indeed, the siHmgpi-induced knockdown of *Hmgpi* expression downregulated *Cdx2* in trophectodermal cells and *Oct4* and *Nanog* in ICM cells, with subsequently reduced proliferation of trophectodermal cells and ICM-derived cells during blastocyst outgrowth.

Genes indispensable for derivation of ES cells

Like *Hmgpi*, *Zscan4* is another exclusively zygotic gene not expressed at any other developmental stage (13). *Zscan4* is a putative transcription factor harboring a SCAN domain and zinc finger domains, and transcribed not only in preimplantation embryos but also in ES cells (13). Reduction of *Zscan4* by RNA interference showed a phenotype similar to that induced by *Hmgpi* knockdown: developmental deterioration at the preimplantation stages, especially cleavage pause at 2-cell stage, and failure in blastocyst outgrowth, ES-cell derivation and implantation. Thus, a preimplantation-specific gene expression pattern could indicate a function in ES-cell derivation and/or maintenance. Indeed, *Hmgpi* was also expressed in entire ES colonies, whereas *Zscan4* shows a peculiar mosaic expression pattern in undifferentiated ES cell colonies. Furthermore, the *Hmgpi* gene is highly expressed in ES cells, but not in EC cells; *Hmgpi* is thus eligible as a putative ECAT (ES cell-associated transcript), whose ESTs are overrepresented in cDNA libraries from ES cells compared with those from somatic tissues and other cell lines including EC cells (34). It is also likely that *Hmgpi* is expressed in iPS cells, based on *in silico* analyses of expression profiles [NCBI GEO database, e.g. GSE10806 (35)]. Thus, *Hmgpi* is likely to have a role in maintaining pluripotent cells, since the ECATs such as *Nanog*, *Eras* and *Gdf3* are required for pluripotency and proliferation of ES cells (34,36,37). In the current study, *Hmgpi* was indeed involved in blastocyst outgrowth of ICM cells. On the other hand, several genes including ECAT members have been implicated in trophectodermal development as well as in early embryonic development. Like *Hmgpi* that was expressed in both ICM cells and trophectodermal cells, *Dnmt3l/Ecat7* has a role in embryonic and extra-embryonic tissues in early developmental stages. *DNMT3L* is recruited by *DNMT3A2* to chromatin (38) to function in DNA methylation in ES cells, and defects in maternal *DNMT3L* induce a differentiation defect in the extra-embryonic tissue (39). The reduced CDX2 expression in blastocysts and poor BrdU incorporation during blastocyst outgrowth following siHmgpi knockdown suggested the potential involvement of *Hmgpi* in trophectodermal development.

In summary, *Hmgpi* is required early on in mammalian development to generate healthy blastocysts that implant successfully and produce ES cells. HMGPI translocates into the nucleus from cytoplasm at the blastocyst stage, which is importantly a turning point of early embryonic development when DNA-methylation levels are at their lowest and implantation takes place. The nuclear HMGPI in blastocysts and ES cells is expected to act as a transcription factor to regulate gene expression networks underlying the generation, self-renewal and maintenance of pluripotent cells. Because E7 embryos have already stopped expressing *Hmgpi*, it is likely

that *Hmgpi* stage-specifically regulates a set of genes that drive peri-implantation development. It will be valuable to identify both cofactors that bind HMGPI and recognize specific DNA sequences, as well as genes that are regulated by *Hmgpi* using ES cells. A better understanding of the *Hmgpi* transcriptional network will also improve culture methods for healthy blastocysts and for generating, maintaining and differentiating ES cells.

MATERIALS AND METHODS

Identification of the mouse *Hmgpi* gene by *in silico* analysis

Preimplantation-specific genes were identified based on global gene expression profiling of oocytes and preimplantation embryos (3,40) and expressed sequence tag (EST) frequencies in the Unigene database. SMART (19) was used for domain prediction analysis. Orthologous relationships between HMG family genes were identified from phylogenetic-tree amino acid sequences determined by a sequence distance method and the Neighbor Joining (NJ) algorithm (41) using Vector NTI software (Invitrogen, Carlsbad, CA, USA).

Collection and manipulation of embryos

Six- to 8-week-old B6D2F1 mice were superovulated by injecting 5 IU of pregnant-mare serum gonadotropin (PMS; Calbiochem, La Jolla, CA, USA) followed by 5 IU of human chorionic gonadotropin (HCG; Calbiochem) 48 h later. The Institutional Review Board of the National Research Institute for Child Health and Development, Japan granted ethics approval for embryo collection from the mice. Unfertilized eggs were harvested 18 h after the HCG injection by a standard published method (42), and the cumulus cells were removed by incubation in M2 medium (EmbryoMax M-2 Powdered Mouse Embryo Culture Medium; Millipore, Billerica, MA, USA) supplemented with 300 μg/ml hyaluronidase (Sigma-Aldrich, St Louis, MO, USA). The eggs were then thoroughly washed, selected for good morphology and collected. Fertilized eggs were also harvested from mated superovulated mice in the same way as unfertilized eggs and embryos with two pronuclei (PN) were collected to synchronize *in vitro* embryo development. Fertilized eggs were cultured in synthetic oviductal medium enriched with potassium (EmbryoMax KSOM Powdered Mouse Embryo Culture Medium; Millipore) at 37°C in an atmosphere of 95% air/5% CO_2. Cultured blastocysts were transferred into pseudopregnant recipients as described previously (42). We transferred 3.5 dpc blastocysts into the uteri of 2.5 dpc pseudopregnant ICR female mice. RNA interference experiments were carried out by microinjecting <10 pl (25 ng/μl) of oligonucleotides (siHmgpi and siControl) into the cytoplasm of zygotes. The optimal siRNAs were determined by testing different concentrations (5, 10, 25 and 50 ng/μl) of three siRNAs (PE Applied Biosystems, Foster City, CA, USA), resuspended and diluted with the microinjection buffer (Millipore). Their target sequences are listed in Supplementary Material, Table S3. More than 10 independent experiments were performed to study the effect of *Hmgpi* knockdown on preimplantation development and implantation.

Culture of ES cells and blastocyst outgrowth

A mouse ES cell line (B6/129ter/sv line) was first cultured for two passages on gelatin-coated culture dishes in the presence of leukemia inhibitory factor (LIF) to remove contaminating feeder cells. Cells were then seeded on gelatin-coated 6-well plates at a density of $1-2 \times 10^5$/well ($1-2 \times 10^4$/cm^2) and cultured for 3 days in complete ES medium: KnockOut DMEM (Invitrogen) containing 15% KnockOut Serum Replacement (KSR; Invitrogen), 2000 U/ml ESGRO (mLIF; Chemicon, Temecula, CA, USA), 0.1 mM non-essential amino acids, 2 mM GlutaMax (Invitrogen), 0.1 mM beta-mercaptoethanol (2-ME; Invitrogen) and penicillin/streptomycin (50 U/50 μg/ml; Invitrogen). Blastocyst outgrowth experiments were carried out according to a standard procedure (42). In brief, zona pellucidae of blastocysts at 3.5 dpc were removed using acidic Tyrode's solution (Sigma). The blastocysts were cultured individually in the ES medium on gelatinized chamber slides at 37°C in an atmosphere of 5% CO_2. The cultured cells were examined and photographed daily. Alkaline phosphatase activity was measured using a specific detection kit (Vector Laboratories, CA, USA) after 6 days in culture. Four independent experiments were performed.

Immunostaining of oocytes and preimplantation embryos

Samples were fixed in 4% paraformaldehyde (Wako Pure Chemical, Osaka, Japan) with 0.1% glutaraldehyde (Wako) in phosphate-buffered saline (PBS) for 10 min at room temperature (RT), and then permeabilized with 0.5% Triton X-100 (Sigma) in PBS for 30 min. Immunocytochemical staining was performed by incubating the fixed samples with primary antibodies for 60 min, followed by secondary antibodies for 60 min. A polyclonal antibody to mouse HMGPI was raised in rabbits against three synthesized peptides designed according to sequence specificity, homology between mouse and human HMGPI, antigenicity, hydrophilicity and synthetic suitability [(i) CIQGHHDGAQSSRQDFTD, (ii) CMSMSGG RSSKFGRTEQS, (iii) ESPRTVSSDMKFQGC; Medical & Biological Laboratories Co, Nagoya, Japan). The anti-HMPGI was used at 1:300 dilution, followed by Alexa Fluor 546 goat anti-rabbit IgG (Molecular Probes, Invitrogen) as the secondary antibody. The anti-Histone H2B antibody (Medical & Biological Laboratories Co, Nagoya, Japan) was used at 1:300 dilution as positive control of nuclear staining, followed by Alexa Fluor 488 goat anti-mouse IgG (Molecular Probes, Invitrogen) as the secondary antibody. Blastocysts were immunostained using a monoclonal anti-Oct4 antibody (mouse IgG2b isotype, 200 μg/ml; Santa Cruz Biotechnology, Santa Cruz, CA, USA), rabbit polyclonal anti-Nanog antibody (ReproCELL, Tokyo, Japan), mouse monoclonal anti-Cdx2 antibody (CELL MARQUE, Rocklin, CA, USA), mouse monoclonal anti-BrdU antibody (Santa Cruz) and rabbit monoclonal anti-active caspase 3 (Abcam) antibody, all diluted at 1:50–300. The appropriate secondary antibodies (IgG) were diluted at 1:300 and supplied by Molecular Probes/Invitrogen: goat anti-rabbit IgG conjugated with Alexa Fluor 546 and goat anti-mouse IgG(H + L) conjugated with Alexa Fluor 488. The cellular DNA (nuclei) was stained with 4′,6-diamidino-2-phenylindole (DAPI; Wako; diluted

1:300). The cells were then washed with PBS and viewed by laser confocal microscopy (LSM510, Zeiss). For HMGPI immunostaining, all samples were processed simultaneously. The laser power was adjusted so that the signal intensity was below saturation for the developmental stage that displayed the highest intensity and all subsequent images were scanned at that laser power. This allowed us to compare signal intensities for HMGPI expression at different developmental stages. The other molecules in blastocysts and outgrowth were viewed and imaged as for the HMGPI expression.

Immunocytochemistry of blastocyst outgrowths and ES cells

Cultured ES cells and blastocyst outgrowths were fixed with 4% paraformaldehyde for 10 min at 4°C, treated with 0.1% Triton X-100 (Sigma) in PBS for 15 min at RT, and then incubated for 30 min at RT in protein-blocking solution consisting of PBS supplemented with 5% normal goat serum (Dako, Glostrup, Denmark). The samples were then incubated overnight with the primary antibodies to OCT4, HMGPI, BrdU or active caspase 3 in PBS at 4°C. The cells were then extensively washed in PBS and incubated at RT with Alexa Fluor 488 goat anti-mouse IgG1 (anti-OCT4 and anti-BrdU antibodies, diluted 1:300; Molecular Probes) or Alexa Fluor 546 goat anti-rabbit IgG(H + L) (anti-HMGPI and anti-caspase 3 antibodies, diluted 1:300), and nuclei were counterstained with DAPI for 30 min. To prevent fading, cells were then mounted in Dako fluorescent mounting medium (Dako).

Incorporation of bromodeoxyuridine (BrdU)

E3.5 blastocysts and blastocyst outgrowths were cultured for 16 h in KSOM and ES medium, respectively, supplemented with 10 μM BrdU (Sigma). Samples were then fixed in 4% paraformaldehyde for 20 min, washed in PBS and then treated with 0.5 M HCl for 30 min.

RNA extraction and real-time quantitative reverse transcriptase (qRT)–PCR

Embryos for qRT–PCR analysis were collected at 18 h post-hCG and cultured as described above. They were harvested at 0.5, 1.25, 1.75, 2.25, 2.75 and 3.75 dpc to obtain fertilized eggs 2-cell, 4-cell, 8-cell, morula and blastocyst embryos, respectively. Three subsets of 10 and 50 synchronized and intact embryos were transferred in PBS supplemented with 3 mg/ml polyvinylpyrrolidone (PVP) and stored in liquid nitrogen. Total RNA from 10 and 50 embryos was extracted using the PicoPure RNA Isolation Kit (Arcturus, La Jolla, CA, USA). The reverse transcription reaction, primed with polyA primer, was performed using Superscript III reverse transcriptase (Invitrogen) following the manufacturer's instructions. Total RNA isolated was reverse transcribed in a 20 μl volume. The resulting cDNA was quantified by qRT–PCR analysis using the SYBR Green Realtime PCR Master Mix (Toyobo, Osaka, Japan) and ABI Prism 7700 Sequence Detection System (PE Applied Biosystems) as described previously (43). An amount of cDNA equivalent to 1/2 an embryo was used for each real-time PCR reaction with a minimum of three replicates, with no-RT and no-template controls for each gene. Data were normalized against *H2afz* by the ΔΔCt method (44). PCR primers for the genes of *Hmgpi, H2afz* and *Gapdh* were listed in Supplementary Material, Table S4. Calculations were automatically performed by ABI software (Applied BioSystems). For alpha-amanitin studies, fertilized eggs were first harvested at 18 h post-hCG, instead of eggs already advanced to the two-pronucleus stage. After 3 h of incubation, eggs that carried both male and female pronuclei were selected at 21 h post-hCG and randomly assigned to two experimental groups: with and without addition of alpha-amanitin to the culture medium. The eggs were further cultured in KSOM at 37°C in an atmosphere of 5% CO_2 until the specified time point (32, 43 and 54 h post-hCG). Embryos used for alpha-amanitin studies and RNA interference experiments were subjected to qRT–PCR as described for the normal preimplantation embryos.

Immunoblot analysis

Protein samples from embryos were solubilized in Sample Buffer Solution without 2-ME (Nacalai Tesque, Kyoto, Japan), resolved by NuPAGE Novex on Tris-acetate mini gels (Invitrogen), and transferred to Immobilon-P transfer membrane (Millipore). The membrane was soaked in protein blocking solution (Blocking One solution, Nacalai) for 30 min at RT before an overnight incubation at 4°C with primary antibody, also diluted in blocking solution. The membrane was then washed three times with TBST (Tris-buffered saline with 0.1% Tween-20), incubated with a horseradish peroxidase-conjugated secondary antibody (0.04 μg/ml) directed against the primary antibody for 60 min, and washed three times with TBST. The signal was detected by enhanced chemiluminescence (SuperSignal West Dura Extended Duration Substrate, Thermoscientific, Rockford, IL, USA) following the manufacturer's recommendations. The intensity of the band was quantified using NIH Image J software. Briefly, the signal was outlined and the mean intensity and background fluorescence were measured. The specific signal was calculated by dividing the band intensities for HMGPI by those for actin.

Statistical analysis

Differences between groups were evaluated statistically using Student's *t*-test or ANOVA, with P-values < 0.05 considered significant.

SUPPLEMENTARY MATERIAL

Supplementary Material is available at *HMG* online.

ACKNOWLEDGEMENTS

The authors would like to thank Dr Takashi Hiiragi for valuable advice and critical reading of the manuscript.

Conflict of Interest statement. The authors declare that there is no conflict of interest that would prejudice the impartiality of the scientific work.

FUNDING

This work was supported, in part, by Grants-in-Aid from the Japan Society for the Promotion of Science (19591911 to T.H., 21390456 to H.A.), by a National Grant-in-Aid from Japanese Ministry of Health, Labor, and Welfare (H21-001, H20-001 to T.H., H18-004 to H.A. and N.K.) and by a Grant-in-Aid from the Yamaguchi- Endocrine Organization to T.H. Funding to pay the Open Access publication charges for this article was provided by Grants-in-Aid for Young Scientists (B) (21791581 to M.Y.).

REFERENCES

1. DePamphilis, M.L., Kaneko, K.J. and Vassilev, A. (2002) Activation of zygotic gene expression in mammals. DePamphilis, M.L. (ed.), *Advances in Developmental Biology and Biochemistry*, Vol. 12, Elsevier Science, B.V.
2. Latham, K.E. and Schultz, R.M. (2001) Embryonic genome activation. *Front. Biosci.*, **6**, D748–D759.
3. Hamatani, T., Carter, M.G., Sharov, A.A. and Ko, M.S. (2004) Dynamics of global gene expression changes during mouse preimplantation development. *Dev. Cell.*, **6**, 117–131.
4. Takahashi, K. and Yamanaka, S. (2006) Induction of pluripotent stem cells from mouse embryonic and adult fibroblast cultures by defined factors. *Cell*, **126**, 663–676.
5. Hamatani, T., Yamada, M., Akutsu, H., Kuji, N., Mochimaru, Y., Takano, M., Toyoda, M., Miyado, K., Umezawa, A. and Yoshimura, Y. (2008) What can we learn from gene expression profiling of mouse oocytes? *Reproduction*, **135**, 581–592.
6. Ko, M.S., Kitchen, J.R., Wang, X., Threat, T.A., Hasegawa, A., Sun, T., Grahovac, M.J., Kargul, G.J., Lim, M.K., Cui, Y. *et al.* (2000) Large-scale cDNA analysis reveals phased gene expression patterns during preimplantation mouse development. *Development*, **127**, 1737–1749.
7. Okazaki, Y., Furuno, M., Kasukawa, T., Adachi, J., Bono, H., Kondo, S., Nikaido, I., Osato, N., Saito, R., Suzuki, H. *et al.* (2002) Analysis of the mouse transcriptome based on functional annotation of 60,770 full-length cDNAs. *Nature*, **420**, 563–573.
8. Solter, D., de Vries, W.N., Evsikov, A.V., Peaston, A.E., Chen, F.H. and Knowles, B.B. (2002) Fertilization and activation of the embryonic genome. Rossant, J. and Tam, P.P.L. (eds), *Mouse Development: Patterning, Morphogenesis, and Organogenesis.*, Academic Press, San Diego, pp. 5–19.
9. Wang, Q.T., Piotrowska, K., Ciemerych, M.A., Milenkovic, L., Scott, M.P., Davis, R.W. and Zernicka-Goetz, M. (2004) A genome-wide study of gene activity reveals developmental signaling pathways in the preimplantation mouse embryo. *Dev. Cell.*, **6**, 133–144.
10. Wang, S., Cowan, C.A., Chipperfield, H. and Powers, R.D. (2005) Gene expression in the preimplantation embryo: in-vitro developmental changes. *Reprod. Biomed. Online*, **10**, 607–616.
11. Zeng, F., Baldwin, D.A. and Schultz, R.M. (2004) Transcript profiling during preimplantation mouse development. *Dev. Biol.*, **272**, 483–496.
12. Choo, K.B., Chen, H.H., Cheng, W.T., Chang, H.S. and Wang, M. (2001) In silico mining of EST databases for novel pre-implantation embryo-specific zinc finger protein genes. *Mol. Reprod. Dev.*, **59**, 249–255.
13. Falco, G., Lee, S.L., Stanghellini, I., Bassey, U.C., Hamatani, T. and Ko, M.S. (2007) Zscan4: a novel gene expressed exclusively in late 2-cell embryos and embryonic stem cells. *Dev. Biol.*, **307**, 539–550.
14. Kanka, J. (2003) Gene expression and chromatin structure in the pre-implantation embryo. *Theriogenology*, **59**, 3–19.
15. Schultz, R.M. and Worrad, D.M. (1995) Role of chromatin structure in zygotic gene activation in the mammalian embryo. *Semin. Cell Biol.*, **6**, 201–208.
16. Thompson, E.M., Legouy, E. and Renard, J.P. (1998) Mouse embryos do not wait for the MBT: chromatin and RNA polymerase remodeling in genome activation at the onset of development. *Dev. Genet.*, **22**, 31–42.
17. Stros, M., Launholt, D. and Grasser, K.D. (2007) The HMG-box: a versatile protein domain occurring in a wide variety of DNA-binding proteins. *Cell. Mol. Life Sci.*, **64**, 2590–2606.
18. Zhang, Q. and Wang, Y. (2008) High mobility group proteins and their post-translational modifications. *Biochim. Biophys. Acta*, **1784**, 1159–1166.
19. Schultz, J., Milpetz, F., Bork, P. and Ponting, C.P. (1998) SMART, a simple modular architecture research tool: identification of signaling domains. *Proc. Natl Acad. Sci. USA*, **95**, 5857–5864.
20. Mamo, S., Gal, A.B., Bodo, S. and Dinnyes, A. (2007) Quantitative evaluation and selection of reference genes in mouse oocytes and embryos cultured in vivo and in vitro. *BMC Dev. Biol.*, **7**, 14.
21. Hock, R., Furusawa, T., Ueda, T. and Bustin, M. (2007) HMG chromosomal proteins in development and disease. *Trends Cell Biol.*, **17**, 72–79.
22. Svarcova, O., Dinnyes, A., Polgar, Z., Bodo, S., Adorjan, M., Meng, Q. and Maddox-Hyttel, P. (2009) Nucleolar re-activation is delayed in mouse embryos cloned from two different cell lines. *Mol. Reprod. Dev.*, **76**, 132–141.
23. Sanij, E., Poortinga, G., Sharkey, K., Hung, S., Holloway, T.P., Quin, J., Robb, E., Wong, L.H., Thomas, W.G., Stefanovsky, V. *et al.* (2008) UBF levels determine the number of active ribosomal RNA genes in mammals. *J. Cell Biol.*, **183**, 1259–1274.
24. Stefanovsky, V.Y., Pelletier, G., Hannan, R., Gagnon-Kugler, T., Rothblum, L.I., Moss, T., Bazett-Jones, D.P. and Crane-Robinson, C. (2001) An immediate response of ribosomal transcription to growth factor stimulation in mammals is mediated by ERK phosphorylation of UBF DNA looping in the RNA polymerase I enhancesome is the result of non-cooperative in-phase bending by two UBF molecules. *Mol. Cell.*, **8**, 1063–1073.
25. Stefanovsky, V.Y., Pelletier, G., Bazett-Jones, D.P., Crane-Robinson, C. and Moss, T. (2001) DNA looping in the RNA polymerase I enhancesome is the result of non-cooperative in-phase bending by two UBF molecules. *Nucleic Acids Res.*, **29**, 3241–3247.
26. Mais, C., Wright, J.E., Prieto, J.L., Raggett, S.L. and McStay, B. (2005) UBF-binding site arrays form pseudo-NORs and sequester the RNA polymerase I transcription machinery. *Genes Dev.*, **19**, 50–64.
27. Falciola, L., Spada, F., Calogero, S., Langst, G., Voit, R., Grummt, I. and Bianchi, M.E. (1997) High mobility group 1 protein is not stably associated with the chromosomes of somatic cells. *J. Cell Biol.*, **137**, 19–26.
28. Bonaldi, T., Talamo, F., Scaffidi, P., Ferrera, D., Porto, A., Bachi, A., Rubartelli, A., Agresti, A. and Bianchi, M.E. (2003) Monocytic cells hyperacetylate chromatin protein HMGB1 to redirect it towards secretion. *EMBO J.*, **22**, 5551–5560.
29. Wang, H., Bloom, O., Zhang, M., Vishnubhakat, J.M., Ombrellino, M., Che, J., Frazier, A., Yang, H., Ivanova, S., Borovikova, L. *et al.* (1999) HMG-1 as a late mediator of endotoxin lethality in mice. *Science*, **285**, 248–251.
30. Cui, X.S., Shen, X.H. and Kim, N.H. (2008) High mobility group box 1 (HMGB1) is implicated in preimplantation embryo development in the mouse. *Mol. Reprod. Dev.*, **75**, 1290–1299.
31. Payer, B., Saitou, M., Barton, S.C., Thresher, R., Dixon, J.P., Zahn, D., Colledge, W.H., Carlton, M.B., Nakano, T. and Surani, M.A. (2003) Stella is a maternal effect gene required for normal early development in mice. *Curr. Biol.*, **13**, 2110–2117.
32. Gurtu, V.E., Verma, S., Grossmann, A.H., Liskay, R.M., Skarnes, W.C. and Baker, S.M. (2002) Maternal effect for DNA mismatch repair in the mouse. *Genetics*, **160**, 271–277.
33. Hock, R., Scheer, U. and Bustin, M. (1998) Chromosomal proteins HMG-14 and HMG-17 are released from mitotic chromosomes and imported into the nucleus by active transport. *J. Cell Biol.*, **143**, 1427–1436.
34. Mitsui, K., Tokuzawa, Y., Itoh, H., Segawa, K., Murakami, M., Takahashi, K., Maruyama, M., Maeda, M. and Yamanaka, S. (2003) The homeoprotein Nanog is required for maintenance of pluripotency in mouse epiblast and ES cells. *Cell*, **113**, 631–642.
35. Kim, J.B., Zaehres, H., Wu, G., Gentile, L., Ko, K., Sebastiano, V., Arauzo-Bravo, M.J., Ruau, D., Han, D.W., Zenke, M. *et al.* (2008)

Pluripotent stem cells induced from adult neural stem cells by reprogramming with two factors. *Nature*, **454**, 646–650.
36. Levine, A.J. and Brivanlou, A.H. (2006) GDF3, a BMP inhibitor, regulates cell fate in stem cells and early embryos. *Development*, **133**, 209–216.
37. Takahashi, K., Mitsui, K. and Yamanaka, S. (2003) Role of ERas in promoting tumour-like properties in mouse embryonic stem cells. *Nature*, **423**, 541–545.
38. Nimura, K., Ishida, C., Koriyama, H., Hata, K., Yamanaka, S., Li, E., Ura, K. and Kaneda, Y. (2006) Dnmt3a2 targets endogenous Dnmt3L to ES cell chromatin and induces regional DNA methylation. *Genes Cells*, **11**, 1225–1237.
39. Arima, T., Hata, K., Tanaka, S., Kusumi, M., Li, E., Kato, K., Shiota, K., Sasaki, H. and Wake, N. (2006) Loss of the maternal imprint in Dnmt3Lmat-/- mice leads to a differentiation defect in the extraembryonic tissue. *Dev. Biol.*, **297**, 361–373.
40. Pan, H., O'Brien, M.J., Wigglesworth, K., Eppig, J.J. and Schultz, R.M. (2005) Transcript profiling during mouse oocyte development and the effect of gonadotropin priming and development in vitro. *Dev. Biol.*, **286**, 493–506.
41. Saitou, N. and Nei, M. (1987) The neighbor-joining method: a new method for reconstructing phylogenetic trees. *Mol. Biol. Evol.*, **4**, 406–425.
42. Nagy, A., Gertsenstein, M., Vintersten, K. and Behringer, R. (2003) *Manipulating the Mouse Embryo: A Laboratory Manual.*, 3rd edn. Cold Spring Harbor Laboratory.
43. Hamatani, T., Falco, G., Carter, M.G., Akutsu, H., Stagg, C.A., Sharov, A.A., Dudekula, D.B., VanBuren, V. and Ko, M.S. (2004) Age-associated alteration of gene expression patterns in mouse oocytes. *Hum. Mol. Genet.*, **13**, 2263–2278.
44. Falco, G., Stanghellini, I. and Ko, M.S. (2006) Use of Chuk as an internal standard suitable for quantitative RT-PCR in mouse preimplantation embryos. *Reprod. Biomed. Online*, **13**, 394–403.

Genes to Cells

Efficient reprogramming of human and mouse primary extra-embryonic cells to pluripotent stem cells

Shogo Nagata[1,2], Masashi Toyoda[3], Shinpei Yamaguchi[1], Kunio Hirano[1], Hatsune Makino[3], Koichiro Nishino[3], Yoshitaka Miyagawa[4], Hajime Okita[4], Nobutaka Kiyokawa[4], Masato Nakagawa[5], Shinya Yamanaka[5], Hidenori Akutsu[3], Akihiro Umezawa[3] and Takashi Tada[1,2]*

[1]*Stem Cell Engineering, Institute for Frontier Medical Sciences, Kyoto University, 53 Kawahara-cho, Shogoin, Sakyo-ku, Kyoto 606-8507, Japan*

[2]*JST, CREST, 4-1-8 Hon-cho, Kawaguchi-shi, Saitama 332-0012, Japan*

[3]*Department of Reproductive Biology, National Research Institute for Child Health and Development, 2-10-1 Ookura, Setagaya-ku, Tokyo 157-8535, Japan*

[4]*Department of Developmental Biology, National Research Institute for Child Health and Development, 2-10-1 Ookura, Setagaya-ku, Tokyo 157-8535, Japan*

[5]*Center for iPS Cell Research and Application (CiRA), Institute for Integrated Cell-Material Sciences, Kyoto University, 53 Kawaharacho, Shogoin, Sakyo-ku, Kyoto 606-8507, Japan*

Practical clinical applications for current induced pluripotent stem cell (iPSC) technologies are hindered by very low generation efficiencies. Here, we demonstrate that newborn human (h) and mouse (m) extra-embryonic amnion (AM) and yolk-sac (YS) cells, in which endogenous *KLF4/Klf4*, *c-MYC/c-Myc* and *RONIN/Ronin* are expressed, can be reprogrammed to hiPSCs and miPSCs with efficiencies for AM cells of 0.02% and 0.1%, respectively. Both hiPSC and miPSCs are indistinguishable from embryonic stem cells in colony morphology, expression of pluripotency markers, global gene expression profile, DNA methylation status of *OCT4* and *NANOG*, teratoma formation and, in the case of miPSCs, generation of germline transmissible chimeric mice. As copious amounts of human AM cells can be collected without invasion, and stored long term by conventional means without requirement for in vitro culture, they represent an ideal source for cell banking and subsequent 'on demand' generation of hiPSCs for personal regenerative and pharmaceutical applications.

Introduction

Induced pluripotent stem cells (iPSCs) have been generated through nuclear reprogramming of somatic cells via retrovirus or lentivirus-mediated transduction of exogenous reprogramming factors Oct4, Sox2, Klf4 and C-Myc (Yamanaka 2007). This has led to greatly enhanced promise for exploring the causes of, and potential cures for, many genetic diseases, as well as increased promise for regenerative medicine. Improvements in delivery methodology have further facilitated iPSC generation by minimizing the requirement for genetic modification (Feng *et al.* 2009). Notably, generation of genetic modification-free iPSCs with reprogramming proteins (Kim *et al.* 2009; Zhou *et al.* 2009) suggests regenerative medicine with personal iPSCs could soon be realized. However, the markedly low efficiency of iPSC generation, with all adult somatic cell types tested to date, remains problematic (Wernig *et al.* 2008). Technological advancements in this field have mainly been achieved using mouse embryonic fibroblasts (MEFs), in which the efficiency of iPSC generation is 10–100 times higher than that with adult somatic cells (Yu *et al.* 2007; Wernig *et al.* 2008). Therefore, current methods would appear to be less than ideal for generating iPSCs from adult somatic cells.

Communicated by: Fuyuki Ishikawa

**Correspondence*: ttada@frontier.kyoto-u.ac.jp

DOI: 10.1111/j.1365-2443.2009.01356.x

Here, to find nuclear reprogramming-sensitive cells collectable with no risk by physical invasion, we generated iPSCs from human and mouse newborn extra-embryonic membranes, amnion (AM) and yolk sac (YS), which consist huge amounts of discarded cells after birth. Interestingly, the efficiency of mouse iPSC (miPSC) generation from the AM was comparable to that of MEFs by retroviral transduction with *Oct4*, *Sox2*, *Klf4* and *c-Myc*. Importantly, human iPSC (hiPSC) is also efficiently generated from human AM cells. Expression of the endogenous *KLF4/Klf4*, *c-MYC/c-Myc* and *RONIN/Ronin* in human/mouse AM cells may function in facilitating the generation efficiency of iPSCs. The human AM cell, which is conventionally freeze-storable, could be a useful cell source for the generation of pluripotent stem cells including iPSCs mediated by nuclear reprogramming in the purpose of personal regenerative and pharmaceutical cure in the future of infants.

Results

Generation of iPSCs from mouse AM and YS cells

Extra-embryonic membranes, AM (amniotic ectoderm and mesoderm layers) and YS (visceral yolk sac endoderm and mesoderm layers) express a high level of proto-oncogene (Curran *et al.* 1984) which function, at least in part, to maintain and protect the fetus in utero. In E18.5 mouse embryos just before birth, AM and YS can be easily recognized microscopically (Fig. 1a). The membranes were dissected from *Oct4-GFP* (OG)/*Neo-LacZ* (Rosa26) embryos as approximately 5–10 mm^2 sections and digested with collagenase. Isolated cells were cultured for 4–5 days resulting in morphologically heterogeneous populations (Fig. 1a) in which OG expression was undetectable. Approximately 1×10^5 cells were then retrovirally transfected with exogenous Oct4, Sox2, Klf4 and c-Myc (OSKM). After approximately 3 weeks, OG-positive embryonic stem cell (ESC)-like miPSC colonies were picked and expanded without drug selection. All AM (female) and YS (male)-miPSC lines generated here, which closely resembled ESCs in morphology (Fig. 1a), had a $2n = 40$ normal karyotype (data not shown).

Characterization of AM and YS-miPSCs

As with ESCs, all AM- and YS-miPSC colonies were positive for alkaline phosphatase (ALP) (Fig. 1b). Immunohistochemical analyses also demonstrated that the cells were positive for pluripotent cell-specific nuclear proteins Oct4 and Nanog, and the surface glycoprotein SSEA1 (Fig. 1b). Thus, the expression profile of all marker proteins tested in AM and YS-miPSCs was similar to that observed in ESCs.

To examine the global transcription profile of these cells, comparative Affymetrix gene expression microarray analyses were performed between AM cells, YS cells, YS-miPSCs and R1 ESCs (Fig 1c). The global gene expression profile of YS-miPSCs was significantly different from that of YS cells. We detected a similar behavior between AM-miPSCs and AM cells (data not shown). Notably, the profile was similar to that of ESCs (Fig. 1c). Together, the data indicate that significant global nuclear reprogramming had occurred in these cells in response to OSKM transfection. We next applied RT-PCR analysis to gain a more focused transcriptional profile of pluripotent cell-specific marker genes in the induced cells. We found that *Nanog*, *Rex1*, *ERas*, *Gdf3*, *Zfp296* and *Ronin* were expressed in both AM and YS-miPSCs, whereas the AM and YS genes, *Igf1* and *Ccl6* were silenced (Fig. 1c). Notably, *Ronin* was expressed not only in AM and YS-miPSCs but also in the precursor AM and YS cells. To investigate whether the exogenous *Oct4*, *Sox2*, *Klf4* and *c-Myc* genes were silenced by DNA methylation as reported for other iPSCs (Jaenisch & Young 2008) in the AM and YS-miPSCs, we examined expression using gene-specific primer sets designed to distinguish endogenous and exogenous transcripts. In all miPSC lines, the expression of endogenous *Oct4*, *Sox2*, *Klf4* and *c-Myc* was similar to that in R1 ESCs, whereas the exogenous *c-Myc* and *Klf4* were fully silenced in some YS-miPSC clones but not in others (Fig. 1c). Notably, high-level expression of endogenous *Klf4* and *c-Myc* was detected even in AM and YS cells, consistent with the expression of proto-oncogene (Curran *et al.* 1984). Endogenous expression of *Klf4*, *c-Myc* and *Ronin* genes that are involved in maintaining pluripotency may play a key function in enhancing the generation efficiency of miPSCs from AM and YS cells.

Timing and efficiency of miPSC generation

The molecular mechanisms that govern OKSM-induced nuclear reprogramming of somatic cells to iPSCs are poorly understood. It has been demonstrated that activation of endogenous *Oct4* may be a landmark for irreversible epigenetic transition toward

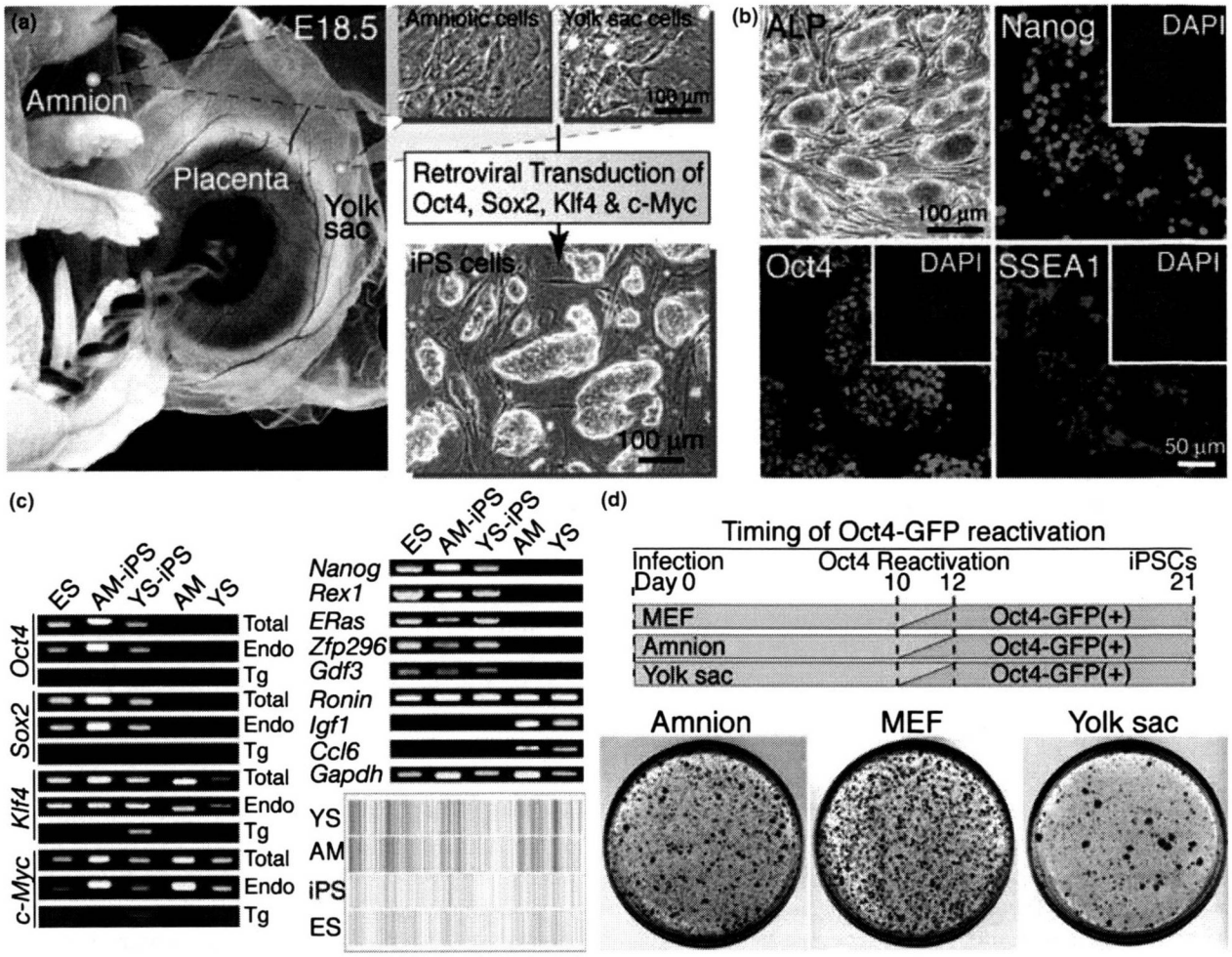

Figure 1 Generation of iPSCs from mouse AM and YS cells. (a) Isolation of AM and YS cells from the extra-embryonic tissues of newborn mice and generation of miPSCs through epigenetic reprogramming by retroviral infection-mediated expression of *Oct4*, *Sox2*, *Klf4* and *c-Myc*. (b) Expression of pluripotent cell marker proteins, alkaline phosphatase (ALP), Nanog, Oct4 and SSEA1. Cell nuclei were visualized with DAPI. (c) Transcriptional activation and silencing of pluripotent and somatic cell marker genes by miPSC induction. RT-PCR analyses revealed that pluripotent marker genes were activated, somatic marker genes were silenced, and *Klf4*, *c-Myc* and *Ronin* were expressed even in AM and YS cells. *Gapdh* is a positive control. Microarray analyses demonstrated global alteration in gene expression profile between YS cells and YS-miPSCs, which more closely resemble mESCs. Relative level of gene expression is illustrated as red > yellow > green. (d) The generation efficiency of ALP-positive colonies and timing of GFP detection demonstrating *Oct4-GFP* reporter gene reactivation. ALP-positive colonies (red) in a 10-cm culture dish was shown when 1.0×10^5 of AM cells, YS cells and MEFs were exposed to OSKM reprogramming factors and reseeded at day 4.

fully reprogrammed iPSCs (Sridharan & Plath 2008). Thus, the timing of reactivation of OG is closely linked with the efficiency of reprogramming. Activation of exogenous OG was detected in some cell populations in every colony around 10 days after OSKM transfection of AM and YS cells, similar to control MEFs examined here and those reported previously (Fig. 1d) (Brambrink *et al.* 2008). The reprogramming efficiency of AM and YS cells was estimated by ALP-staining 21 days after OSKM transfection with reseeding at day 4. Notably, the number of ALP-positive colonies was similar between AM cells (4373 ± 983; mean ± SEM, $n = 3$) and MEFs (4997 ± 1049, $n = 3$), and ~50% in YS cells (2293 ± 487, $n = 3$). Thus, the efficiency of AM reprogramming by OSKM is comparable to that of MEFs, and far exceeds that of adult somatic cells (Fig. 1d).

Germline-transmissible chimeras with AM and YS-miPSCs

To address *in vivo* differentiation potential of the AM and YS-miPSCs, approximately 10 agouti miPSCs were microinjected into C57BL/6J × BDF1 blastocysts (black), and transferred into white ICR foster mothers to generate chimeras. Three male YS-miPSC and two female AM-miPSC lines were tested for chimera formation. X-gal staining analysis on sections of E15.5 embryos demonstrated successful generation of normally developing chimeric embryos with OG/*Neo-LacZ* miPSC contribution to the majority of tissues in all miPSC lines examined (data not shown). We next examined the miPSC potential for normal growth to sexual maturity and germline transmission. Two high-degree chimeric mice with a YS-miPSC line and three high-degree chimeric mice with two AM-miPSC lines, characterized by the >50% contribution of agouti coat color (Fig. 2a), developed normally into adulthood. However, an adult YS-miPSC chimera developed a neck tumor around 8–10 weeks after birth, which may be due to reactivation of the exogenous *c-Myc* as reported previously (Nakagawa *et al.* 2008). Testes isolated from affected males were bisected and one-half was X-gal-stained for LacZ activity whereas the other half was cryosectioned. Blue staining in the seminiferous tubule indicated that YS-miPSCs could contribute to germ cell development. To confirm this, testis cryosections immunohistochemically stained with antibodies against LacZ (iPSC-derived cell marker) and TRA98 (spermatogonia and spermatocyte marker) (Fig. 2b). Germ cells in all tubules were positive for TRA98, whereas germ cells in only some seminiferous tubules were positive for LacZ, clearly demonstrating that YS-miPSCs are capable of contributing to the differentiating germ line in chimeras. Finally, to examine whether the genetic information of YS-miPSCs was transmissible to the next generation, DNA isolated from progeny of the remaining YS-miPSC chimera was analyzed by genomic PCR with a primer set specific to *Neo*. Seven of the thirty-five pups examined were positive, demonstrating that YS-miPSCs are able to differentiate into fully functional germ cells (Fig. 2c). In one of three female AM-miPSC chimeric mice, competence for contribution to germ cells was detected by X-gal staining analysis of ovaries (data not shown).

Teratoma formation with AM and YS-miPSCs

The differentiation competence of AM and YS-miPSCs was further tested by teratoma formation induced by injection of cells into the inguinal region of immunodeficient SCID mice. Teratomas were isolated 5–8 weeks after for histological analysis and for gene expression analysis. Hematoxylin–eosin (HE) staining of paraffin sections demonstrated that the three primary layers were generated as morphologically shown by ectodermal glia and neuroepithelium, mesodermal muscle and endodermal ciliated epithelium and cartilage (Fig. 2d). Multi-lineage differentiation of miPSCs was verified by transcription of endodermal, mesodermal and ectodermal genes in the majority of teratomas (Fig. 2e).

Generation of iPSCs from human AM cells

To examine whether hiPSCs could be efficiently generated from primary AM cells isolated from the amniotic membrane (~100 cm^2) of the placenta of newborn human (Fig. 3a), the reprogramming factors *OCT4*, *SOX2*, *KLF4* and *c-MYC* were introduced by vesicular stomatitis virus G glycoprotein (VSV-G) retroviral transduction. About 20 AM-hiPSC lines were established from 1.0×10^5 AM cells infected (0.02%). The efficiency of AM-hiPSC generation is markedly high relative to that with cells from human adult tissues (Yu *et al.* 2007). AM-hiPSCs were morphologically similar to human ESCs (hESCs) (Fig. 3a). Immunohistochemical analyses demonstrated expression of the pluripotent cell-specific nuclear proteins OCT4, SOX2 and NANOG, and the keratan sulfate proteoglycan TRA-1-60 (Fig. 3b) consistent with the profile observed in hESCs. To extend this analysis, we examined the expression profile of genes by RT-PCR. The endogenous reprogramming factor genes *OCT4*, *SOX2*, *KLF4* and *c-MYC* were all activated in AM-hiPSCs, whereas the transgenes were fully silenced (Fig. 3c). Expression of pluripotent cell-specific genes *NANOG, REX1, GDF3, ESG1, FGF4, TERT* and *RONIN* were also activated in all AM-hiPSC clones consistent with the profile of control hESCs (Fig. 3c). Notably, transcription of *KLF4, c-MYC,* and *RONIN* was detected not only in AM-hiPSCs but also AM cells. Similar to mouse AM and YS cells, endogenous expression of *KLF4, c-MYC* and *RONIN* in human AM cells may facilitate acquisition of reprogramming competency for efficient generation of hiPSCs.

DNA methylation of OCT4 and NANOG in AM-hiPSCs

To further characterize the pluripotent nature of AM-hiPSCs, the promoter CpG methylation status

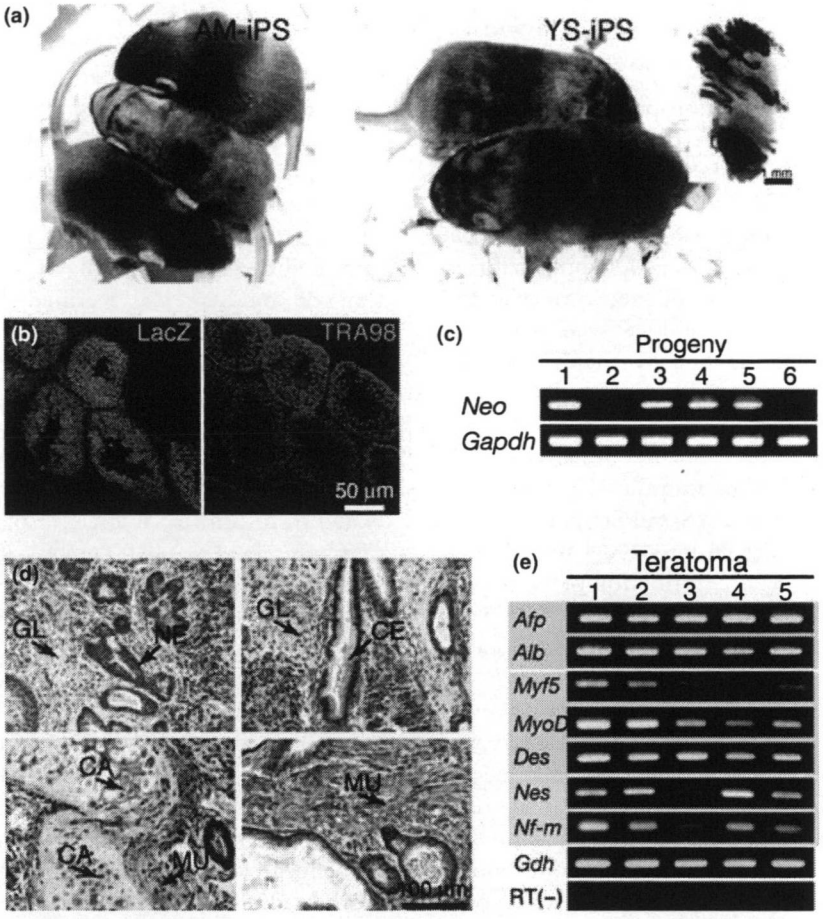

Figure 2 Pluripotency of AM and YS-miPSCs. (a) Chimeric mice with female AM-miPSCs and male YS-miPSCs. Inset: X-gal staining of testis collected from an adult YS-miPSC chimera (blue cells are YS-miPSC derivatives). (b) Immunohistochemical double staining of testis cryosections from a YS-miPSC chimera with anti-LacZ (YS-miPSC-derived germ cells) and anti-TRA98 (spermatogonia and spermatocytes) antibodies. (c) Genotyping of progeny obtained by backcrossing with YS-miPSC chimeras. *Neo* positive demonstrates germline transmission of YS-miPSC genetic information. *Gapdh* is positive control. (d) Hematoxylin-eosin staining of teratoma sections generated by AM and YS-miPSC implantation. GL, glia (ectoderm); NE, neuroepithelium (ectoderm); CE, ciliated epithelium (endoderm); CA, cartilage (ectoderm); MU, muscle (mesoderm). (e) Transcription analysis of lineage-specific genes in teratomas generated with AM and YS-miPSCs. Gray rectangle: endoderm makers; purple rectangle: mesoderm markers; pink rectangle: ectoderm markers. *Afp*, *α-Fetoprotein*; *Alb*, *albumin*; *Des*, *desmin*; *Nes*, *Nestin*; *Nf-m*, *neurofilament-M*; *Gdh*, *Gapdh* (positive control).

of key pluripotency genes was examined by bisulfite-modified DNA sequencing. Promoters of both *OCT4* and *NANOG* were found to highly methylated in hAM cells, consistent with transcriptional silencing in these cells. Conversely, both promoter regions were hypo-methylated in AM-hiPSCs consistent with the observed reactivation (Fig. 3d). These data demonstrate that human AM cells are capable of being epigenetically reprogrammed to AM-hiPSCs through forced expression of reprogramming factors.

Teratoma formation with AM-hiPSCs

To address whether the AM-hiPSCs have competence to differentiate into specific tissues, teratoma formation was induced by implantation under the kidney capsule of immunodeficient nude mice. Twenty-one out of twenty-four AM-hiPS independent clones induced teratoma formation within 6–10 weeks of implantation (1.0×10^7 cells/site). Histological analysis by HE staining of paraffin-embedded sections demonstrated that the three

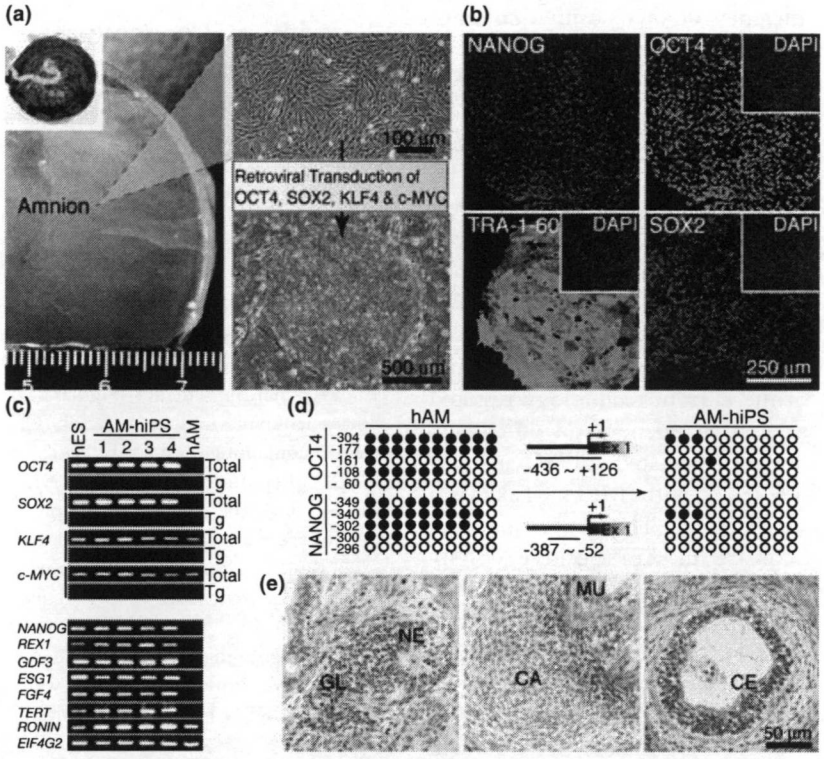

Figure 3 Generation of iPSCs from human AM cells. (a) Isolation of hAM cells from extra-embryonic tissues of human newborns and generation of hiPSCs through epigenetic reprogramming by retroviral infection-mediated expression of *OCT4*, *SOX2*, *KLF4* and *c-MYC*. (b) Expression of pluripotent cell marker proteins, NANOG, OCT4, TRA-1-60 and SOX2. Cell nuclei were visualized with DAPI. (c) Transcriptional activation of pluripotent marker genes by hiPSC induction. RT-PCR analyses revealed that the exogenous *OCT4*, *SOX2*, *KLF4* and *c-MYC* genes were silenced and the endogenous pluripotent marker genes were activated in AM-hiPSCs. *KLF4*, *c-MYC* and *RONIN* were expressed even in hAM cells before reprogramming. *EIF4G2* (*eukaryotic translation initiation factor 4 gamma 2*) is included as a positive control. (d) Epigenetic reprogramming of the *OCT4* and *NANOG* promoter regions. Bisulfite-modified DNA sequence analysis demonstrated a transition from hyper-methylation in AM cells (black circles) to hypo-methylation in AM-hiPSCs (white circles). (e) Hematoxylin-eosin staining of teratoma sections of teratoma generated by AM-hiPSC implantation. GL, glia (ectoderm); NE, neuroepithelium (ectoderm); CE, ciliated epithelium (endoderm); CA, cartilage (ectoderm); MU, muscle (mesoderm).

primary layers were generated as shown by ectodermal glia and neuroepithelium, mesodermal muscle and endodermal ciliated epithelium and cartilage morphologically (Fig. 3e). Thus, the majority of AM-hiPSC clones have potential for multi-lineage differentiation *in vivo*.

Discussion

We here demonstrated that hiPSCs and miPSCs were efficiently generated from newborn AM cells, in which endogenous *Klf4*, *c-Myc* and *Ronin* were highly expressed. The generation efficiency of miPSCs from AM cells was comparable to that from MEFs in mice and was notably high to that from adult somatic cells in humans. The properties of AM-hiPSCs and AM or YS-miPSCs resemble those of fully reprogrammed iPSCs from other tissues and ESCs.

iPSCs are generated through epigenetic reprogramming of somatic cells. Information on the base sequence of DNA in nuclei is unchanged through the reprogramming, although the gene expression profile is altered through the reprogramming from the somatic cell to the iPSC type. Developmentally rewound iPSCs retain aged DNA base sequence information inherited from somatic cells. The base sequence of DNA accumulates mutations through aging with cell division and mis-repair. Young somatic cells are suitable for iPSC generation rather than aged somatic cells. Therefore, it is suggested that the AM cells accumulating less genetic mutation are safer than the adult somatic cells as a cell source for iPSC generation.

The generation efficiency of OG-positive colonies was approximately four times lower than that of ALP-positive colonies and it is likely that miPSC generation will be further reduced (Wernig *et al.* 2008). Furthermore, when pre-iPSCs are reseeded, the generation efficiency of iPSC outcome could be roughly estimated as $1/2^X$ (X = reseeded day after infection or transfection; doubling time of pre-iPSC is estimated as 24 h). Recently, iPSC generation technology has been developed and improved with MEFs and human embryonic or newborn fibroblasts (HNFs) as representative somatic cells. Even with these types of cells, application of the current technology resulted in a marked decrease in iPSC generation efficiency. The retroviral transduction-mediated miPSC generation efficiency is 0.05–0.1% with MEFs (Takahashi *et al.* 2007; Wernig *et al.* 2007). The generation efficiency of hiPSCs (~0.01% in ALP-positive colony and 0.0025% in hiPSC outcome) (Yu *et al.* 2007; Wernig *et al.* 2008) is ~10 times lower than that of miPSCs. The generation efficiency of genetic modification-free hiPSCs from HNFs by direct delivery of reprogramming proteins is estimated at about 0.001% in outcome (Kim *et al.* 2009). Notably, it is evident that the generation of hiPSCs from adult somatic cells is much harder than that from MEFs. In fact, analysis with a secondary dox-inducible transgene system shows that the efficiency varies between different somatic cell types (Wernig *et al.* 2008). Thus, for practical application of iPSC technology to medical care, identification of reprogramming-sensitive cell types is a key issue. Human primary keratinocytes are one candidate cell type for efficient generation of hiPSCs from adult patients (the efficiency of ALP-positive colony = 1.0%) (Aasen *et al.* 2008). Here, we have shown that human and mouse AM cells, in which the endogenous *KLF4/Klf4*, *c-MYC/c-Myc* and *RONIN/Ronin* are naturally expressed, are highly reprogramming-sensitive (hiPSC generation efficiency was approximately 0.02% in outcome). An important point is that relatively huge amounts of human AM cells can be collected from discarded AM membranes at birth with no risk to the individual. Furthermore, these cells can be kept in long-term storage without requirement for amplification by in vitro cell culture.

Our findings illustrate that human AM cells are a strong candidate cell source for collection and banking that could be retrieved on demand and used for generating personalized genetic modification-free iPSCs applicable for clinical treatment and drug screening.

Experimental procedures

Amnion and yolk sac cells

In mice, AM and YS membranes collected from E18.5 embryos from GOF-18/delta PE/GFP (Oct4-GFP) transgenic females (Yoshimizu *et al.* 1999) mated with 129/Rosa26 transgenic males (Friedrich & Soriano 1991) were digested with 0.1% collagenase (Wako, Osaka, Japan) and 20% fetal bovine serum (FBS) at 37 °C for 1 h, and then repeatedly passed through a 26-gauge needle. The cell suspension was cultured with mES medium (DMEM/F12 (Dulbecco's modified Eagle's medium/Ham's F12) (Wako) supplemented with 15% FBS, 10^{-4}M 2-mercaptoethanol (Sigma) and 1000 U/mL of recombinant leukemia inhibitory factor (Chemicon, Temecula, CA, USA) containing 5 ng/mL basic fibroblast growth factor (bFGF) (Peprotech, Rocky Hill, NJ, USA). Following culture for 2–3 days, the adherent AM and YS cells growing to near-confluence were applied for iPSC experiments.

In humans, the AM membrane was cut into tiny pieces with dissection scissors. The AM membrane pieces were cultured in DMEM with 10% FBS for 7–10 days. The adherent AM cells growing to near-confluence were applied for iPSC experiments. Primary AM cells were provided from the cell bank of RIKEN Bioresource Center, Japan.

Generation of iPSCs

In mouse, each of pMXs-Oct4, Sox2, Klf4, c-Myc and DsRed (an indicator of retroviral silencing) was transfected into the Plat-E cells using the FuGENE6 Transfection Reagent (Roche Diagnostics, Indianapolis, IN, USA). A 1 : 1 : 1 : 1 : 4 mixture of Oct4, Sox2, Klf4, c-Myc and DsRed retroviruses in supernatants with 4 μg/mL polybrene (Nacalai Tesque, Kyoto, Japan) was added to AM and YS cells at 1.0×10^5 cells per 3 cm well. At day 4 after infection, the cells were reseeded into a 10 cm culture dish on feeder cells with mES medium. Colonies were picked around day 20.

In humans, pMXs-OCT4, SOX2, KLF4 or c-MYC, pCL-GagPol, and pHCMV-VSV-G vectors were transfected into 293FT cells (Invitrogen, Carlsbad, CA, USA) using the TransIT-293 reagent (Mirus). A 1 : 1 : 1 : 1 mixture of OCT4, SOX2, KLF4 and c-MYC viruses in supernatant with 4 μg/mL polybrene were added to AM cells at 1.0×10^5 cells per 3 cm well. The cells were subcultured on feeder cells into a 10 cm dish with the iPSellon medium (Cardio) supplemented with 10 ng/mL bFGF (Wako) (hES medium). Colonies were picked up around day 28.

Immunocytochemistry

Human and mouse cells were fixed with 4% paraformaldehyde in phosphate-buffered saline (PBS) for 10 min at 4 °C. After washing with 0.1% Triton X-100 in PBS (PBST), the cells were prehybridized with blocking buffer for 1–12 h at 4 °C and then incubated with primary antibodies; anti-SSEA4

Table 1 Primers for RT-PCR and PCR

Gene name	5′-Forward-3′	5′-Reverse-3′
Mice		
Oct4 (total)	CTGAGGGCCAGGCAGGAGCACGAG	CTGTAGGGAGGGCTTCGGGCACTT
Oct4 (endogenous)	TCTTTCCACCAGGCCCCCGGCTC	TGCGGGCGGACATGGGGAGATCC
Oct4 (transgene)	CCCATGGTGGTGGTACGGGAATTC	AGTTGCTTTCCACTCGTGCT
Sox2 (total)	GGTTACCTCTTCCTCCCACTCCAG	TCACATGTGCGACAGGGGCAG
Sox2 (transgene)	CCCATGGTGGTGGTACGGGAATTC	TCTCGGTCTCGGACAAAAGT
Klf4 (total)	CACCATGGACCCGGGCGTGGCTGCCAGAAA	TTAGGCTGTTCTTTTCCGGGGCCACGA
Klf4 (endogenous)	GCGAACTCACACAGGCGAGAAACC	TCGCTTCCTCTTCCTCCGACACA
Klf4 (transgene)	CCCATGGTGGTGGTACGGGAATTC	GTCGTTGAACTCCTCGGTCT
c-Myc (total)	CAGAGGAGGAACGAGCTGAAGCGC	TTATGCACCAGAGTTTCGAAGCTGTTCG
c-Myc (endogenous)	CAGAGGAGGAACGAGCTGAAGCGC	AAGTTTGAGGCAGTTAAAATTATGGCTGAAGC
c-Myc (transgene)	CTCCTGGCAAAAGGTCAGAG	GACATGGCCTGCCCGGTTATTATT
Nanog	ATGAAGTGCAAGCGGTGGCAGAAA	CCTGGTGGAGTCACAGAGTAGTTC
Eras	CAAAGATGCTGGCAGGCAGCTACC	GACAAGCAGGGCAAAGGCTTCCTC
Gdf3	AGTTTCTGGGATTAGAGAAAGC	GGGCCATGGTCAACTTTGCCT
Rex1	GACATCATGAATGAACAAAAAATG	CCTTCAGCATTTCTTCCCTG
Zfp296	AAGCACCCAGATCTGTTGACCT	GAGCCTCTGGGGTATCTAGG
Ronin	GCCTCAGAGCTAGAGGCTGCTACG	TGGAAGGAGTCACGAATTCTGCAG
Igf1	GGACCAGAGACCCTTTGCGGGG	GGCTGCTTTTGTAGGCTTCAGTGG
Cdl6	CCTAAGCACCCTGAAGCAAG	ACAACTGGGAACCCACAAAGC
Gapdh	CCCACTAACATCAAATGGGG	CCTTCCACAATGCCAAAGTT
α-Fetoprotein	TCGTATTCCAACAGGAGG	CACTCTTCCTTCTGGAGATG
Albumin	AAGGAGTGCTGCCATGGTGA	CCTAGGTTTCTTGCAGCCTC
Myf-5	TGCCATCCGCTACATTGAGAG	CCGGGTAGCAGGCTGTGAGTTG
MyoD	GCCCGCGCTCCAACTGCTCTGAT	CCTACGGTGGTGCGCCCTCTGC
Desmin	TTGGGGTCGCTGCGGTCTAGCC	GGTCGTCTATCAGGTTGTCACG
Nestin	GGAGTGTCGCTTAGAGGTGC	TCCAGAAAGCCAAGAGAAGC
Neurofilament-M	GCCGAGCAGACCAAGGAGGCCATT	CTGGATGGTGTCCTGGTAGCTGCT
Neo	CGGCAGGAGCAAGGTGAGAT	CAAGATGGATTGCACGCAGG
Humans		
OCT4 (total)	GCCGTATGAGTTCTGTGG	TCTCCTTCTCCAGCTTCAC
SOX2 (total)	TAAGTACTGGCGAACCATCT	AAATTACCAACGGTGTCAAC
KLF4 (total)	ACTCGCCTTGCTGATTGTCT	GAACGTGGAGAAAGATGGGA
c-MYC (total)	GCGTCCTGGGAAGGGAGATCCGGAGC	TTGAGGGGCATCGTCGCGGGAGGCTG
NANOG	ATTATGCAGGCAACTCACTT	GATTCTTTACAGTCGGATGC
REX1	CAGATCCTAAACAGCTCGCAGAAT	GCGTACGCAAATTAAAGTCCAGA
GDF3	CTTATGCTACGTAAAGGAGCGGG	GTGCCAACCCAGGTCCCGGAAGTT
ESG1	ATATCCCGCCGTGGGTGAAAGTTC	ACTCAGCCATGGACTGGAGCATCC
FGF4	CTACAACGCCTACGAGTCCTACA	GTTGCACCAGAAAAGTCAGAGTTG
TERT	CCTGCTCAAGCTGACTCGACACCGTG	GGAAAAGCTGGCCCTGGGGTGGAGC
RONIN	CACTGTAGACAGCAGTCAGG	TGCCTTTCATCTCTTTCATC
EIF4G2	AAGGAAAGGGACTGAGTTTC	CCAAGAAAGCTTCTTCTTCA
Bis-OCT4	GATTAGTTTGGGTAATATAGTAAGGT	ATCCCACCCACTAACCTTAACCTCTA
Bis-NANOG	TGGTTAGGTTGGTTTTAAATTTTTG	AACCCACCCTTATAAATTCTCAATTA

(1 : 300) (Chemicon), anti-TRA-1–60 (1 : 300) (Chemicon), anti-Oct4 (1 : 50) (Santa Cruz Biotechnology, Santa Cruz, CA, USA), anti-Nanog (1 : 300) (ReproCELL, Tokyo, Japan), anti-Sox2 (1 : 300) (Abcam, Cambridge, UK) and/or anti-SSEA1 (1 : 1000) (DSHB) antibodies for 6–12 h at 4 °C. They were incubated with secondary antibodies; anti-rabbit IgG, anti-mouse IgG or anti-mouse IgM conjugated with Alexa 488 or 546 (1 : 500) (Molecular Probes, Eugene, OR, USA) in blocking buffer for 1 h at room temperature. The cells were counterstained with 4,6-diamidino-2-phenylindole (DAPI) and then mounted with a SlowFade light antifade kit (Molecular Probes). To examine germline competence,